HHS Public Access

Author manuscript

*Cell Rep*. Author manuscript; available in PMC 2023 January 09.

Published in final edited form as:

*Cell Rep*. 2022 November 22; 41(8): 111675. doi:10.1016/j.celrep.2022.111675.

# Dynamic quality control machinery that operates across compartmental borders mediates the degradation of mammalian nuclear membrane proteins

**Pei-Ling Tsai**[1], **Christopher J.F. Cameron**[1,2], **Maria Fernanda Forni**[3], **Renee R. Wasko**[3], **Brigitte S. Naughton**[1], **Valerie Horsley**[3], **Mark B. Gerstein**[1,4,5,6], **Christian Schlieker**[1,7,8,*]

[1]Department of Molecular Biophysics and Biochemistry, Yale University, New Haven, CT 06511, USA

[2]Department of Radiology and Biomedical Imaging, Yale University, New Haven, CT 06520, USA

[3]Department of Molecular, Cellular and Developmental Biology, Yale University, New Haven, CT 06511, USA

[4]Program in Computational Biology and Bioinformatics, Yale University, New Haven, CT 06511, USA

[5]Department of Computer Science, Yale University, New Haven, CT 06511, USA

[6]Department of Statistics and Data Science, Yale University, New Haven, CT 06511, USA

[7]Department of Cell Biology, Yale School of Medicine, New Haven, CT 06520, USA

[8]Lead contact

## SUMMARY

Many human diseases are caused by mutations in nuclear envelope (NE) proteins. How protein homeostasis and disease etiology are interconnected at the NE is poorly understood. Specifically, the identity of local ubiquitin ligases that facilitate ubiquitin-proteasome-dependent NE protein turnover is presently unknown. Here, we employ a short-lived, Lamin B receptor disease variant as a model substrate in a genetic screen to uncover key elements of NE protein turnover. We identify the ubiquitin-conjugating enzymes (E2s) Ube2G2 and Ube2D3, the membrane-resident ubiquitin ligases (E3s) RNF5 and HRD1, and the poorly understood protein TMEM33. RNF5, but not HRD1, requires TMEM33 both for efficient biosynthesis and function. Once synthesized, RNF5 responds dynamically to increased substrate levels at the NE by departing from the endoplasmic reticulum, where HRD1 remains confined. Thus, mammalian protein quality control machinery



*Correspondence: christian.schlieker@yale.edu.

AUTHOR CONTRIBUTIONS

Conceptualization, P.T. and C.S.; methodology, P.T. and C.S.; software, C.J.C.; formal analysis, P.T. and C.J.C.; investigation, P.T., M.F.F., R.R.W., and B.N.; writing – original draft, P.T. and C.S.; writing – review and editing, P.T., B.N., and C.S.; visualization, P.T. and C.S.; supervision, V.H., M.B.G., and C.S.; funding acquisition, C.S.

DECLARATION OF INTERESTS

The authors declare no competing interests.

SUPPLEMENTAL INFORMATION

Supplemental information can be found online at https://doi.org/10.1016/j.celrep.2022.111675.

partitions between distinct cellular compartments to address locally changing substrate loads, establishing a robust cellular quality control system.

## In brief

Mutations in nuclear membrane proteins cause many human diseases. While several of those affect protein stability, the mechanisms of protein quality control at the mammalian nuclear envelope remain to be elucidated. Using a functional genomic approach, Tsai et al. identify a dynamic machinery that targets misfolded nuclear membrane proteins for degradation.

## Graphical abstract

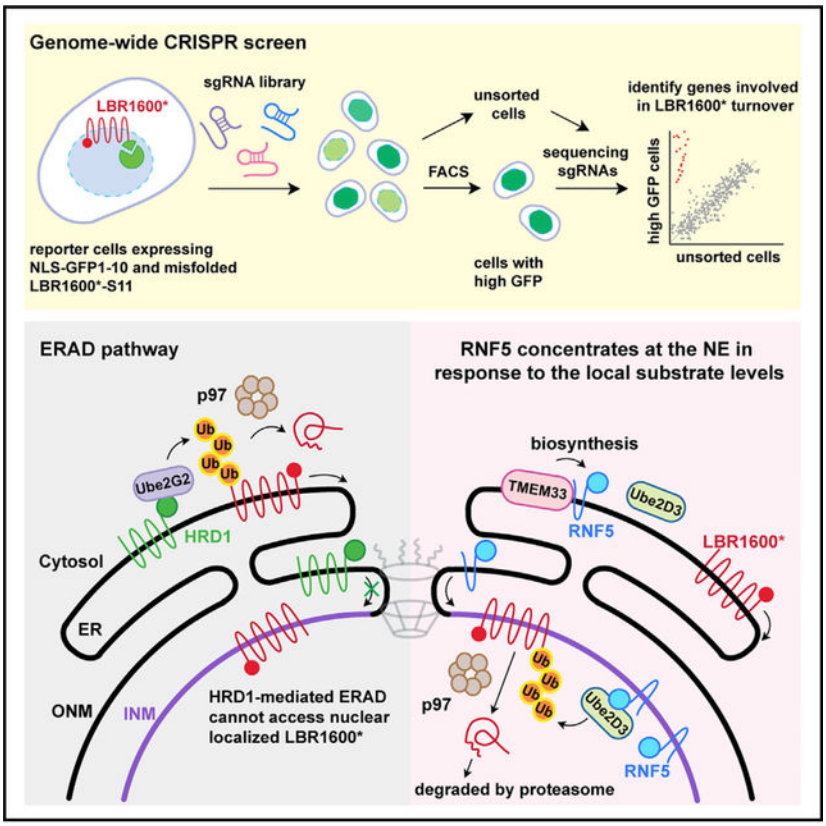


Highlights

## INTRODUCTION

The nuclear envelope (NE) is a highly dynamic membrane system and a defining feature of eukaryotes. While the NE is a subcompartment of the contiguous endoplasmic reticulum (ER), a wide range of physiological processes, including mechanical stress management, integration of cell signaling, regulation of gene expression, and critical elements of lipid synthesis, are carried out at the NE.[1–3] Several of these functions are perturbed in human pathologies, many of which arise from mutations in NE-resident proteins.[4] One critical yet poorly understood facet of NE dynamics is the process of protein homeostasis. Both

the identity and the underlying molecular mechanisms responsible for protein folding and turnover in the contiguous ER are increasingly well understood.[5,6] However, our understanding of analogous processes in the NE of mammalian cells has only started to emerge recently,[7,8] with major elements of NE turnover still remaining uncharacterized.[1,9,10]

Despite the membrane continuity of the ER with the outer nuclear membrane (ONM) and inner nuclear membrane (INM) (Figure 1A), larger multiprotein complexes involved in ER-associated degradation (ERAD) cannot simply diffuse to the INM. The physical nature of this ONM/INM diffusion barrier—presumably imposed by the nuclear pore complex (NPC)-pore membrane interface—has remained mysterious, despite major advances in our understanding of NPC structure. However, it is evident that proteins with larger structured cytosolic domains cannot gain access to the INM.[11–13] This raises the question of whether a dedicated INM-resident machinery exists that may perform a role that is similar to that of the ERAD machinery. First insights into this problem were obtained in *Saccharomyces cerevisiae*. Here, the E3 ubiquitin (Ub) ligases Doa10 and the Asi complex are key elements of an ERAD-equivalent process at the INM termed INM-associated degradation (INMAD).[14–17] Our gap in understanding analogous processes in mammalian cells, and in particular E3s capable of exploring INM territory, is in large part due to the lack of suitable short-lived (model) substrates that have been key for the identification and characterization of ERAD machinery.

We have previously reported that a subset of Lamin B receptor (LBR) mutations responsible for Pelger-Huët anomaly and the fatal condition Greenberg skeletal dysplasia render this INM protein metabolically unstable, perturbing its essential role as a sterol reductase during cholesterol synthesis.[7] One of these disease alleles, termed LBR1600*, gives rise to a short-lived, truncated LBR variant carrying seven substituted nucleotides near the C terminus resulting in a premature stop codon.[7,18,19] Based on these findings, we employed the split-GFP system[20] to circumvent the diffusion barrier that would arise by fusing full-length GFP to INM proteins.[21,22] The resulting model substrate, termed LBR1600*S11, carries only the last beta strand of GFP (S11) fused to its C terminus. Upon stabilization through blocking of machinery involved in LBR1600*S11 turnover, this model substrate can accumulate and complement GFP 1–10 (lacking S11) that is directed to the nucleoplasm by virtue of a nuclear localization signal, allowing for the detection of GFP fluorescence as a measure for LBR1600*S11 turnover[21](Figure 1A).

In this study, we employ this reporter system as a readout for a genome-wide, CRISPR-Cas9-based screen aimed at identifying LBR1600* turnover machinery. The most robust candidates that emerged from this screen include the E2 ubiquitin-conjugating enzymes Ube2G2 and Ube2D3, as well as the E3 Ub ligases RNF5 and HRD1. Moreover, we identified the highly conserved, yet poorly understood, polytopic membrane protein TMEM33. By combining imaging modalities and biochemical characterization in HeLa cells, we show that ER- and INM-resident E3s establish a two-layered defense system against misfolded proteins, with only RNF5 being able to access the nuclear compartment. RNF5 responds to increased substrate levels at the INM by rapid relocalization from the ER to the nuclear compartment to counteract local protein misfolding. Last, a series of genetic epistasis experiments allow us to place TMEM33 in one pathway with RNF5, but not with

HRD1. Our functional characterization allows us to deduce that TMEM33 has a dual role. TMEM33 is required at a post-transcriptional step for efficient RNF5 biosynthesis but also for RNF5 function. In sum, we identified RNF5 as an E3 ligase that can dynamically explore ER and INM territory, creating a robust defense system that can readily react to local changes of substrate load. The results add to an increasingly dynamic picture of cellular protein homeostasis and advance our understanding of congenital disorders affecting the stability of NE-resident proteins.

## RESULTS

### Generation and validation of a stable cell line expressing split-GFP fused reporters

LBR1600* is a short-half-life protein residing in the INM and the ER. Upon proteasomal inhibition, LBR1600* accumulates in the nucleoplasm, while blocking VCP/p97 activity results in the accumulation of LBR1600* in the NE.[7] These properties are mirrored by LBR1600*S11, demonstrating that neither the distribution of LBR1600*S11 nor its degradation are altered by the added beta strand.[21] Since VCP/p97 is required to extract ubiquitylated proteins from membranes,[23,24] it seems reasonable to suggest that p97 extracts LBR1600* directly from the INM following its ubiquitylation through an as-yet unknown, presumably NE-resident E3 ligase.

To systematically identify factors involved in INM protein degradation, we employed our previously established readout[21] with an improved split-GFP system[20] to construct a reporter for a genome-wide CRISPR screen. To this end, we used the tetracycline-controlled Tet-on system to introduce the reporters LBR1600*S11 and NLS-GFP1-10 into our established LBR knockout (KO) cell line[7] via retroviral transduction, followed by the isolation of a clonal cell line. The reporters were induced to express in the presence of doxycycline. We will henceforth refer to the resulting cell line as the reporter cell line.

Our rationale was that, if LBR1600*S11 was stabilized due to the CRISPR-Cas9-mediated depletion of factors required for INM protein turnover, LBR1600*S11 would accumulate, resulting in higher GFP fluorescence upon association with NLS-GFP1-10 in the nucleus. To test whether the designed reporter cell line can be used in conjunction with fluorescence-activated cell sorting (FACS), we examined the dynamic range of GFP fluorescence in our reporter cell line using flow cytometry in the presence or absence of CB-5083, a compound that inhibits the ATPase activity of VCP/p97.[25] Indeed, our fluorescent reporter yielded a robust, doxycycline-dependent shift of the cell population to a higher fluorescence that was further increased upon inhibition of VCP/p97 by nearly one order of magnitude (Figure 1B). Given the obvious signal shift upon blocking p97, an established LBR1600* turnover factor,[7] we conclude that our engineered cell line is well suited for a FACS-based CRISPR-Cas9 screen.

### A genome-wide CRISPR screen identifies factors involved in LBR1600* turnover

We transduced our reporter cell line with a lentiviral Brunello KO library targeting to 19,114 genes with four single guide RNAs (sgRNAs) per gene and 1,000 non-targeting sgRNA controls. The sgRNAs of the library have been optimized to improve the targeting efficiency

with lower off-target effects.[26] About 3% of cells with the highest GFP fluorescence were enriched via two rounds of FACS sorting at day 8 and day 13 post transduction (Figure 1C). The resulting sgRNA sequences within these populations were analyzed using high-throughput sequencing. Gene ranks were generated by comparing the gene enrichment in the cell population with the highest GFP fluorescence versus the unsorted population using the MAGeCK algorithm,[27] followed by application of a modified robust rank aggregation algorithm (α-RRA)[28] (Figure 1D; Table S1). Among the top-ranked candidates, we identified several genes that are known to be involved in the Ub/proteasome and ERAD pathways. These include the E3 ligases RNF5 and SYVN1/HRD1, the HRD1-interacting protein SEL1L,[29] and the ubiquitin-conjugating enzymes Ube2G2 and Ube2D3. Thus, our screen indeed captured genes with relevance to protein quality control. In addition, TMEM33, a poorly understood ER-resident membrane protein that has been tied to ER morphology,[30] calcium homeostasis,[31,32] lipid homeostasis,[33] and the STING (stimulator of interferon genes) signaling pathway,[34,35] was also identified among the top-scoring genes. Interestingly, Pom33, the yeast homolog of TMEM33, has previously been tied to ER morphology and NPC distribution.[36–38] In addition to the genes presumably involved in LBR1600*S11 turnover, our screen also identified factors that bear on the reporter biosynthesis such as genes that are linked to RNA metabolism, transcriptional regulation, and nonsense-mediated decay (NMD)[39] (Figures 1D and S1A–S1D for Gene Ontology [GO] term enrichment analysis). In the following we will focus our analysis on genes or gene products related to our primary objective: the identification of protein turnover machinery in the mammalian NE.

As a first step toward target validation, we engineered polyclonal KO cells for RNF5, HRD1/SYVN1, SEL1L, Ube2G2, Ube2D3, and TMEM33 by transducing our reporter cell line with vectors expressing three independent sgRNAs targeting each of these six genes (two for SEL1L) (see Figure S1E for validation). Compared with the control transduced with a non-targeting sgRNA, cells with sgRNAs targeting RNF5, Ube2G2, and Ube2D3 showed a major increase in GFP fluorescence (Figure 2A). HRD1, TMEM33, and SEL1L KO cells also exhibited higher GFP fluorescence, although somewhat less pronounced compared with RNF5 KO. Overall, the impact of each gene depletion was highly consistent across three independent sgRNAs for the same target, indicating that our candidate validation recapitulated the results of the genome-wide screen.

To exclude the possibility of off-target effects, we performed rescue experiments with cDNAs specifying RNF5, Ube2G2, Ube2D3, HRD1, or TMEM33, using LBR1600*S11 immunofluorescence as readout. Expression of wild-type (WT) RNF5 in RNF5 KO cells led to a selective disappearance of the LBR1600*S11 signal in transfected cells, but not in untransfected cells in the same field of view, consistent with a role of RNF5 in LBR1600*S11 turnover (Figures 2B and 2C). However, overexpression of a RNF5 ligase-inactive mutant carrying a C42A mutation in the RING domain barely influenced substrate levels, suggesting that the E3 ligase activity of RNF5 is required for LBR1600*S11 degradation (Figure 2B, cf. upper and lower panel). Similar rescue effects were also observed when we expressed Ube2G2, Ube2D3, and TMEM33 proteins in the respective KO cells, consistently resulting in a decrease in LBR1600*S11 levels (Figures 2B and 2C). In contrast, overexpression of WT HRD1 into HRD1 KO cells only led to a partial rescue,

and the transfected cells still had detectable LBR1600 levels within the nucleus (Figure 2B, panel 3). Overexpression of a HRD1 ligase-inactive mutant C291A had no effect on rescuing the degradation of LBR1600*S11 (Figure 2B, panel 4). These results hint at the possibility that LBR1600*S11 can be degraded via at least two distinct pathways. We hypothesize that a subset of LBR1600*S11 is recognized by the HRD1 ligase at the ER and dislocated into the cytoplasm via the canonical ERAD pathway; however, if LBR1600*S11 escapes the ERAD system and is trafficked to the nucleus by virtue of the N-terminal topogenic moiety[40] that is unperturbed by the mutation, HRD1 can no longer act on it.

Re-expression of RNF5, TMEM33, Ube2G2, and Ube2D3 in the respective KO cells led to barely detected LBR1600 signals (a.u. < 5) in the transfected cells, consistent with a restoration of LBR1600*S11 degradation. Collectively, these rescue experiments confirm that the candidates that emerged from the CRISPR screen are involved in controlling LBR1600*S11 levels.

## RNF5 and HRD1 mediate the degradation of LBR1600*S11

We next asked whether these validated candidates indeed affect LBR1600*S11 turnover. To this end, we performed cycloheximide (CHX) chase assays in which translation was blocked at time zero, allowing us to monitor protein degradation over 2 h. Under normal conditions, LBR1600* has a half-life of about 15–20 min[7] (Figure 3A). All individual KO cell lines showed a significant delay in LBR1600*S11 turnover compared with control cells (Figures 3A and 3B). Among these, RNF5 KO has the strongest effect on LBR1600*S11 degradation, with a resulting increase in half-life to about 2 h. KO of Ube2G2 and Ube2D3 resulted in an increase of the half-life of LBR1600*S11 to 1 h, and KO of TMEM33 and HRD1 exhibited a modest increase in half-life to 45 min (Figures 3A and 3B). Since our reporter cell line is based on an LBR KO background to facilitate the detection of the LBR1600*S11 via anti-LBR antibodies in imaging-based assays, we performed analogous turnover experiments in LBR WT cells expressing HA-LBR1600*. Here we arrived at virtually identical observations (Figures S6C and S6D), arguing against a major contribution of the endogenous LBR locus in this context.

Notably, none of the single-gene KOs in either genetic background exhibit complete LBR1600*S11 stabilization, suggesting functional redundancy. To test this possibility directly, we depleted the E3 ligase HRD1 via small interfering RNA (siRNA) in a RNF5 KO background. Indeed, the combined perturbation showed a more pronounced effect on LBR1600*S11 degradation than the individual RNF5 KO (Figures 3C and 3D). Taken together, these data indicate that both RNF5 and HRD1 are involved in LBR1600*S11 turnover and are part of distinct pathways.

## RNF5 is required for LBR1600*S11 polyubiquitylation through the K48 linkage type

Since most validated candidates have ubiquitin-directed activities, we next tested whether their depletion had a direct impact on the polyubiquitylation of LBR1600*S11. We transfected the indicated KO cells (see Figure 4A) with HA-ubiquitin (Ub) and immunoprecipitated the LBR1600*S11, expressed via doxycycline induction. As expected, KO of E3 ligases RNF5 and HRD1, or E2 enzymes Ube2G2 and Ube2D3, impaired

the ubiquitylation of LBR1600*S11 (Figure 4A). Interestingly, KO of TMEM33 also led to an apparent decrease in LBR1600*S11 ubiquitylation. Similar results were obtained upon HA-LBR1600* expression in cells harboring an LBR WT locus when samples were boiled prior to immunoprecipitation to avoid non-specific association of unrelated ubiquitylated proteins (Figure S6A). Since RNF5 KO has the strongest effect on LBR1600*S11 degradation, we next asked whether overexpression of RNF5 could promote the ubiquitylation of LBR1600*S11. FLAG-RNF5 and HA-Ub were co-transfected into cells expressing LBR1600*S11 and ubiquitylation of LBR1600*S11 was analyzed after immunoprecipitation. Cells overexpressing RNF5 clearly displayed an increase in ubiquitylation of LBR1600*S11 (Figure 4B). This increase was not observed in cells overexpressing the RING-type E3 ligases TRIM25 and RNF121, which we included as specificity controls, even though these are expressed at equivalent or higher levels, respectively (Figure 4B). To further characterize which Ub linkage was used by RNF5, we transiently transfected cells stably expressing LBR1600*S11 with FLAG-RNF5 and either WT HA-Ub or a mutant derivative in which only one specific lysine residue is available for chain formation. The highest level of ubiquitylation was observed in cells expressing K48-only (K48O) Ub, while an intermediate level of ubiquitylation was observed in the case of K33O and K63O Ub (Figure S2A).

Next, we performed analogous experiments with HA-Ub derivatives carrying individual mutations in acceptor lysine residues. Consistent with our previous data, overexpression of a Ub K48R mutant derivative exhibited the most pronounced reduction of Ub modification, particularly in the high molecular mass range corresponding to polyubiquitylation (Figure S2B). Since the LBR1600*S11 ubiquitylation in the above experiments employing RNF5 overexpression is primarily dependent on RNF5 (Figure S2, cf. lanes 1 and 2), we deduce from our data that RNF5 expression primarily results in LBR1600*S11 polyubiquitylation through the K48-linkage type that is responsible for proteasomal turnover.[41]

Finally, we asked whether RNF5 associates with its substrates. To avoid overexpression artifacts, we introduced a C-terminal HA tag at the endogenous RNF5 locus in our reporter cell via CRISPR/Cas12a-mediated PCR tagging.[42] Specific integration was validated via immunoblotting and RNF5 depletion using siRNA, which effectively depleted the HA-reactive band that migrated at the expected molecular mass of 25 kDa (Figure 4C). We compared cells expressing LBR1600*S11 with non-induced cells, both in the absence and presence of MG132, with our parent cell line harboring an unmodified RNF5 locus as additional control. Detergent lysates were subjected to immunoprecipitation with anti-HA antibodies, followed by immunoblotting with an LBR-specific antibody. As expected, LBR1600*S11 was only detected in lysates of induced samples. In anti-HA immunoprecipitates, LBR1600*S11 was most abundant in samples derived from induced cells in presence of MG132, consistent with LBR1600*S11 stabilization (Figure 4D). Thus, we conclude that LBR1600*S11 is associated with RNF5.

## TMEM33 can be placed in one pathway with RNF5, but not with HRD1

We next asked whether a functional relationship exists between TMEM33, RNF5, and HRD1. First, we transiently transfected FLAG-RNF5 and HRD1-myc into our reporter

cell line or KO derivatives, allowing a side-by-side comparison of LBR1600*S11 levels in non-transfected and transfected cells in the same field of view. As expected, RNF5 overexpression resulted in a clear reduction of LBR1600*S11 in control cells (Figure 5A, first panel). In contrast, we did not observe reduced LBR1600*S11 levels in a TMEM33 KO background upon RNF5 overexpression, suggesting that RNF5 and TMEM33 act in one pathway, or are at least functionally connected (Figure 5A, cf. panel 1 and 2). This effect was not observed when HRD1 transfectants were compared, which displayed a moderate reduction in LBR1600 levels irrespective of the genetic TMEM33 background (Figure 5A, cf. third and fourth panels and Figure 5B). Furthermore, overexpressing RNF5 in HRD1 KO cells results in a disappearance of LBR1600*S11, suggesting that these E3s act independently and RNF5 activity alone is sufficient for clearing up the substrate in the INM (Figure 5A, last panel, and Figure 5B). These observations proved robust when larger sample sizes (n = 100) were analyzed (Figure 5B).

Having deduced that RNF5 and TMEM33 are functionally connected by genetic means, we next asked whether a physical interaction exists between these proteins. We transiently transfected our reporter cell line with TMEM33-HA and FLAG-RNF5 WT or RNF5 C42A in the presence or absence of LBR1600*S11 induction, followed by immunoprecipitation using HA antibodies. Both FLAG-RNF5 WT and C42A mutant were co-precipitated with TMEM33-HA, and this interaction was independent of the presence of LBR1600*S11 (Figure 5C, cf. lane 3 and 4 and lane 5 and 6). In addition, LBR1600*S11 also co-precipitated with FLAG-RNF5 and TMEM33-HA, suggesting a multimeric complex exists *in vivo* (Figure 5C, cf. lanes 3 and 4).

Finally, we performed an additional epistasis analysis by comparing the degradation of LBR1600*S11 in control and TMEM33 KO cells combined with siRNAs for further depleting RNF5 or HRD1. As described above (Figure 3), deletion of TMEM33 led to a stabilization of LBR1600*S11 with an increase in half-life from 20 to 50 min. However, depleting RNF5 in TMEM33 KO cells led to no additive effect on LBR1600*S11 turnover; instead, we observed a slight decrease in half-life to 40 min, which might be attributed to the compensation of HRD1 or other pathways while the RNF5 is depleted. In contrast, combining TMEM33 KO with HRD1 depletion results in a pronounced increase in half-life to approximately 2 h (Figures 5D and 5E). Taken together with our imaging analysis, which follows the same trend but with even more pronounced effects (Figures 5A and 5B), we deduce that RNF5 and TMEM33 are functionally linked, while TMEM33 and HRD1 act independently from each other and hence their combined perturbation leads to an additive stabilizing effect.

### TMEM33 deletion reduces cellular RNF5 levels

To further characterize the functional TMEM33-RNF5 relationship, we compared RNF5 levels in WT and TMEM33 KO cells in a CHX-chase experiment. We observed a strong reduction of RNF5 levels in TMEM33 KO cells compared with WT cells in all time points, but without significant turnover of RNF5 during the chase period (Figure 6A). This finding suggests that RNF5 is either extremely short lived in TMEM33 KO (leading to very low levels already at the zero time point) or that the reduced levels are due to changes in RNF5

transcription or translation. We first asked whether RNF5 transcript levels were reduced in TMEM33 KO cells. We did not observe reduced RNF5 transcript levels in TMEM33 KO cells compared with WT cells as judged by qPCR analysis (Figure 6B). To test whether the translation of RNF5 mRNA is affected, we subjected cytosolic homogenates obtained from WT and TMEM33 KO cells to a polysome profiling analysis that assesses the number of ribosomes associated with a given mRNA[43] (Figures 6C and 6D). Unexpectedly, we did not observe significant differences in the distribution of RNF5 mRNA levels in fractions derived from WT or TMEM33 KO cells (Figure 6D), indicating that similar numbers of ribosomes are associated with RNF5 mRNA in WT and TMEM33 KO backgrounds. To validate that the mRNAs quantified along the gradient indeed associate with polysomes rather than co-migrating messenger ribonucleoproteins (mRNPs), we included EDTA in a parallel experiment to dissociate ribosomal subunits. As expected, we observed a light-density shift of the RNF5 mRNA (Figure 6D, upper panel). Similar effects were observed for GAPDH mRNA and 28S/18S ribosomal RNAs, which we monitored as additional controls (Figures 6C and 6D, lower panel). Finally, we examined the abundance of several ER membrane proteins (HRD1, RNF185, sec61β) and soluble proteins (GAPDH and hnRNPA1). Except for RNF5 showing a pronounced reduction in protein level in TMEM33 KO, none of these proteins displayed significant differences in TMEM33 KO versus WT controls (Figure 6E, cf. Figure S6B for an analogous experiment in LBR WT cells). Thus, the TMEM33 KO specifically affects RNF5, ruling out global translational defects in TMEM33 KO cells.

Since ribosome association of RNA does not always correlate with the production of a polypeptide,[44] we employed $^{35}$S-based pulse-chase analysis to evaluate the translational efficiency of RNF5 mRNA and protein stability. To this end, we transiently transfected the reporter cell line and TMEM33 KO cells with plasmids encoding FLAG-RNF5 and monitored the metabolic stability after a short (5 min) labeling. Compared with WT, TMEM33 KO showed a pronounced reduction of FLAG-RNF5 at time zero (t = 0). However, RNF5 was metabolically unstable in both WT and TMEM33 KO cells (Figure 6F), possibly due to autoubiquitination, which is at times observed upon overexpression of E3s.[45] We therefore additionally analyzed the ligase-inactive RNF5 C42A mutant. Indeed, this variant was stable in either genetic background; however, it also displayed lower levels at the zero time point in TMEM33 KO cells compared with WT cells (Figure 6G).

While we cannot exclude the formal possibility RNF5 is rapidly turned over during the short (5 min) pulse period in absence of TMEM33, we can conclude that TMEM33 is required for the efficient biosynthesis of RNF5, revealing a hitherto unknown activity of this protein.

## Substrate-induced trafficking of RNF5 to the INM

One major remaining question is whether RNF5 can access the INM. As overexpression of INM-resident membrane proteins often results in non-authentic ER localization, we tagged RNF5 at the endogenous locus of HeLa WT cells using a C-terminal HA tag. RNF5-HA mainly displayed a punctate staining in the cytoplasm with strong enrichment at the ER, as judged by co-localization with Sec61β and TMEM33 (Figure 7A). We did not note a specific enrichment in the NE compared with the ER in the original images, although a

smaller subset of RNF5 foci did co-localize with LBR, which we used as an NE marker (Figure 7A, see inset).

We next asked whether the RNF5 localization can be altered depending on the presence of the substrate. To this end, we employed our reporter cell line, in which RNF5 was tagged at the endogenous locus (Figure 4C). In the absence of doxycycline, RNF5 again displayed a diffuse cytosolic pattern with ER enrichment (Figure 7B, top panel). However, upon induction of the LBR1600*S11 transgene, RNF5-HA efficiently relocalized to the NE, where we observed a high degree of co-localization with its substrate, LBR1600*S11 (Figure 7B, bottom panels and Figure S7 for an analogous experiment in LBR WT cells). This observation is further confirmed by electron microscopy in conjunction with immunogold labeling. In the absence of LBR1600*S11 induction, RNF5 was rarely found in the nucleus (Figures S3A and S3B). However, more RNF5 localized in the nucleus or close to the INM upon expression of LBR1600*S11 (Figures S3A and S3B). This is consistent with our immunofluorescence data and supports the idea that the RNF5 responds to the change of local substrate levels and alters its localization. Taken together, we conclude that RNF5 can partition between the ER and nuclear membrane compartments, whereas HRD1 is confined to the ER.

## RNF5 depends partly on Ube2D3, while HRD1 relies on Ube2G2 for LBR1600* degradation

Finally, we asked which E2 enzyme works with RNF5. To this end, we overexpressed FLAG-RNF5 in the reporter cell line carrying deletions of either Ube2G2 or Ube2D3 as well as control cells and examined whether the RNF5 still functions in LBR1600* degradation while one of the specific E2s was deleted. Overexpression of RNF5 in control cells resulted in the anticipated disappearance of LBR1600*S11, and this effect was reproduced when Ube2G2 was deleted, suggesting Ube2G2 is dispensable for RNF5-dependent LBR1600*S11 degradation (Figures S4A and S4B, cf. data plots 2 and 4). In contrast, overexpression of RNF5 in Ube2D3 KO cells displayed a moderate decrease in LBR1600*S11 level, indicating RNF5 requires Ube2D3 for efficient LBR1600*S11 degradation (Figures S4A and S4B, cf. data plots 2 and 6). This effect is not fully penetrant suggesting that other E2 enzymes that remain to be identified might be able to compensate for the absence of Ube2D3. This result is completely opposite when HRD1 transfectants were compared. Ube2G2 deletion abolishes HRD1's function on LBR1600* turnover, whereas overexpressing HRD1 in Ube2D3 KO results in a similar reduction in LBR1600* level compared with the expression in control cells, indicating that HRD1 primarily uses Ube2G2 as E2 enzyme for LBR1600* degradation (Figures S4C and S4D).

Since Ube2G2 and Ube2D3 are small soluble proteins (~15–20 kDa), we next examined whether the E2 enzymes also alter their localization in response to the substrate expression. To avoid protein mislocalization caused by overexpression, we introduced the HA tag at the endogenous locus of Ube2G2 and Ube2D3. Endogenous Ube2G2 mainly exhibits an ER/cytosolic staining, while Ube2D3 mostly resides in the nucleoplasm with minor staining in the cytosol (Figures S5A and S5B top panel). For either E2, we found that the localization was essentially unchanged regardless of the presence of LBR1600*S11 (Figure S5). However, we note that the distinctive localization of both E2s is conducive for driving

the ubiquitylation of LBR1600* in conjunction with HRD1 and RNF5 in the ER and INM, respectively.

## DISCUSSION

In this study, we reveal a bipartite surveillance mechanism that mammalian cells utilize to coordinate the turnover of misfolded INM proteins. Using a LBR disease variant as readout for a genetic screen, we identified RNF5 and HRD1 as the major Ub ligases responsible for the INM protein turnover (Figures 1 and 3). As a first line of defense, the canonical ERAD pathway involving HRD1 removes newly synthesized, misfolded INM proteins (see Figure 7C for a model). However, similar to the Hrd1p in yeast,[16] HRD1 cannot act on INM-resident substrates. Even when overexpressed, HRD1 cannot completely reduce LBR1600*S11 levels, whereas RNF5 overexpression eliminates LBR1600*S11 quantitatively even in HRD1-deficient cells (Figures 5A and 5B). Correspondingly, we did not detect HRD1 in nuclear fractions (Figure S3C). This is presumably because HRD1 participates in large, ER-resident protein complexes[5,6,9,46,47] that prohibit HRD1 diffusion to the INM. This raises the question of how misfolded INM proteins that escaped the ERAD system are degraded.

We report that, at the INM, a second surveillance mechanism is at work, operated by the E3 ligase RNF5 (Figures 7B and 7C). RNF5 has been reported to participate in ERAD and engage a variety of substrate proteins, including the cystic fibrosis transmembrane conductance regulator (CFTR)[48] and SREBP-cleavage activating protein (SCAP).[33,49] RNF5 has also been linked to innate immunity activation via mediating the degradation of mitochondrial antiviral signaling protein (MAVS)[50] and STING.[51] Thus, most RNF5 functions have been reported to occur outside of the nuclear compartment. We demonstrate, however, that RNF5 localizes not only to the ER but also to the INM (Figures 7B and S3). Surprisingly, this dynamic localization of RNF5 appears to be related to substrate concentration at the INM as the induction of LBR1600*S11 results in a pronounced relocalization from the ER to the NE (Figure 7B).

We hypothesize that this dynamic system has several advantages compared with an E3 ligase that is firmly anchored to the INM by association with the nuclear lamina or associated proteins. First, RNF5 is comparatively small (molecular mass [MW], 19.9 KDa) and therefore below the size limit that separates ER and INM membrane into distinct territories. Consequently, large membrane areas can be surveilled effectively to readily identify clients for ubiquitylation, either to initiate the degradation of misfolded proteins or activate proteins in the context of regulatory proteolysis. Second, RNF5 can dynamically respond to local changes in substrate concentration in distinct membrane compartments via diffusion to areas of substrate accumulation. The latter property might be particularly important in mammalian cells where NE proteomes fluctuate due to mitotic NE breakdown and reassembly in open mitosis and beyond.[1,52]

Interestingly, a recent study using yeast as model system suggested that folded but unassembled subunits of protein complexes at the ER membrane are not degraded by ERAD. Instead, these orphan subunits traffic to the INM where they are targeted for

degradation by the Asi complex which is—in distinction to RNF5—always present at the INM irrespective of substrate fluctuations.[53–55] Taken together with our results, it thus appears that both substrates and the E3s that act on them can partition between cellular compartments, increasing robustness of the cellular protein quality-control network. The observation that RNF5 partitions into the nuclear compartment also suggests that additional functions outside of protein quality control might exist. Indeed, a recent study implicated RNF5 in modulating epigenetic modifications in the context of acute myeloid leukemia.[56] Thus, further studies are warranted to unearth additional connections to nuclear processes.

In addition to the E3s, we also identified the poorly understood membrane protein TMEM33 in our screen (Figure 1). By combining a genetic epistasis analysis (Figures 5A, 5B, and 5D) with biochemical approaches (Figure 5C), we deduce that TMEM33 forms a functional pair uniquely with RNF5, but not with HRD1. Recently, TMEM33 and RNF5 proteins were implicated in lipid homeostasis.[33] How are these proteins functionally connected? We observed that both the steady-state levels and the *de novo* synthesis levels of RNF5 are strongly reduced in TMEM33 KO cells compared with WT cells (Figures 6A, 6E, and 6F). This effect was specific to RNF5, as the levels of other ER-membrane-resident E3s were unaffected (Figure 6E). Since we observed neither differences in RNF5 mRNA levels nor differences in polysome association of the RNF5 transcript in TMEM33 KO (Figures 6B and 6D), we deduce that TMEM33 is required for an early, post-transcriptional step in RNF5 biosynthesis. For example, TMEM33 might play a role in membrane insertion of RNF5. The polysomes associated with RNF5 mRNAs in TMEM33 KO might reflect stalled translation intermediates. Additional experiments will be necessary to scrutinize this process in the future and may identify other proteins whose biosynthesis also depends on TMEM33.

Given the observation that RNF5 levels are strongly reduced in TMEM33 KO cells, we attempted to overexpress RNF5 and examined whether the expressed protein can restore the defect in LBR1600* turnover caused by TMEM33 deletion. However, simply overexpressing RNF5 was not sufficient to restore substrate turnover in TMEM33 KO. Instead, we observed an increase in substrate accumulation (Figures 5A and 5B). We speculate that this increase reflects a non-productive, dominant negative interaction of RNF5 with its substrate in the absence of TMEM33, making LBR1600* unavailable to the HRD1-dependent degradation pathway acting on LBR1600* in the ER. It will therefore be interesting to explore in the future whether the absence of TMEM33 leads to the production of an aberrant RNF5 variant due to defective biosynthesis. Alternatively, TMEM33 may regulate RNF5 function or participate in a multimeric complex strictly requiring TMEM33 for RNF5 activity.

In conclusion, our results define a dynamic, bipartite quality-control system that maintains the integrity of the mammalian INM. While HRD1 operates in the ER, RNF5/TMEM33 can partition between ER and INM membrane territories (Figure 7C). Thus, local changes in substrate concentration can be readily balanced to increase the overall robustness of cellular quality control. Our study also provides mechanistic insights into ties between nuclear envelopathies and protein homeostasis, defining pharmacological targets for therapeutic development.

### Limitations of the study

In this study, we performed a CRISPR-Cas9 screen to identify genes that mediate INM protein turnover. Due to the nature of the knockout screen, our results do not necessarily capture essential genes that might be underrepresented in our dataset. For example, we have previously assigned VCP/p97 to a key role in the process,[7,21] but p97/VCP did not emerge as a candidate gene in our screen.

While our study identified the machinery that targets a misfolded INM protein for degradation, the same machinery is poised for regulatory proteolysis at the INM under specific physiological conditions. Whether RNF5 has other substrates at the INM and which stimuli are at work for inducing their regulated degradation remain to be elucidated in the future.

## STAR★METHODS

### RESOURCE AVAILABILITY

**Lead contact—**Further information and requests for resources and reagents should be directed to and will be fulfilled by the lead contact, Christian Schlieker (Christian.Schlieker@yale.edu).

**Materials availability—**Materials generated in this study are available upon request to the lead contact without restrictions.

**Data and code availability—**Raw sequencing data of the CRISPR screen have been deposited at Sequence Read Archive (SRA: PRJNA888777) and are available as of the date of publication. Processed CRISPR screen results are available in Table S1.

This study does not report original code. Further information regarding reanalysis of data generated in this study is available upon request to the lead contact.

### EXPERIMENTAL MODEL AND SUBJECT DETAILS

All cell lines used in this study were cultured in DMEM media supplemented with 10% heat-inactivated Fetal Bovine Serum and 100 U/mL penicillin/streptomycin. All cell lines were maintained at 37°C with 5% CO2 and passaged every 3 days. Cell lines were regularly tested for bacterial contamination via Hoechst staining.

### METHOD DETAILS

**Generation of a stable cell line expressing NLS-GFP1-10 and LBR1600*S11—**A split-GFP system[20] was employed to engineer the reporter for the CRISPR screen, in which the C-terminus of LBR1600* was fused with the small fragment of GFP termed S11(TELNFKEWQKAFTDMM) using a linker sequence GGG, and the cells also co-expressed the complementary fragment GFP1-10 tagged with the SV40 nuclear localization sequence PKKKRKV at its N-terminus using a linker sequence GGGSGGGS. To establish the cell line constitutively expressing the transgenes, we used a retroviral vector (Retro-X Tet-On advanced inducible expression system, Takara Bio) to carry the expression genes.

The detailed procedures of producing the retrovirus, transducing the target cells, and isolating the single clonal cell line were performed as described previously[21] with the exception that the puromycin resistance gene of pRetroX-Tight-Pur vector was replaced with a hygromycin resistance gene in order to be compatible with the antibiotic marker of the lentiCRISPR library described later. In brief, the transgenes were cloned into the modified pRetroX-Tight-Hygro vector followed by retrovirus production. LBR KO HeLa cells[7] were seeded in a 6-well plate at a density of $2 \times 10^5$/well and transduced with retroviruses carrying the genes encoding tet repressor, LBR1600*S11, and NLS-GFP1-10. After G418 (800 μg/mL) and hygromycin (60 μg/mL) selection, cells were seeded in 10-cm plates at low density about 50 cells/plate, and grown until the single cluster formed. The isolated single clonal cells were validated by immunofluorescence in the presence and absence of 0.5 μg/mL doxycycline and 10 μM MG132 to confirm the LBR1600*S11 had proper expression and normal distribution. The selected clonal cells were treated with 5 μM p97 inhibitor (CB-5083, APExBIO) for 4 h and analyzed by flow cytometry. Finally, the clonal cell line with the largest dynamic window of GFP intensity was selected for CRISPR screen. Prior to the screen, the clonal cell line was transduced with lentivirus generated using lentiCas9-Blast (Addgene, #52962) to make the cells stably express Cas9 endonuclease.

**Lentivirus production—**For CRISPR/Cas9-mediated knockout screen, we used the human sgRNA library Brunello that comprised total 76441 sgRNAs targeting to 19114 genes[26] (Addgene# 73178, deposited by David Root lab). The detailed protocol for library preparation and sequencing was performed as described.[60] Briefly, the pooled library was amplified by electroporating 100 ng library into 25 μL of electrocompetent cells (Lucigen) and repeated by total 4 replica. After electroporation, 1 mL of pre-warmed recovery medium was immediately added, and the cells were transferred to a culture tube. The tubes were filled with media up to 8 mL and split into two aliquots, shake at 32°C for 1 h, and spread onto 15-cm plates with 0.5 mL/plate. The bacteria were grown at 32°C for 16–18 h, and plasmids were extracted using Plasmid Maxi kit (Qiagen) following manufacturer's protocol. To avoid overloading the column resulting in a loss of library representation, we applied only 0.45 gram of bacteria pellet into each Maxiprep purification and used a total of 15 columns for the entire extraction. An aliquot of the pooled plasmids was analyzed using deep sequencing to ensure the library had >90% representation.

For the library virus production, low-passage HEK293T cells were seeded in 15 × 15-cm plates with 12 million cells/plate the day before transfection. After 24 h, each plate was co-transfected with 33 μg lentiGuide-puro vectors carrying the Brunello library, 5 μg envelope vector pMD2.G (Addgene# 12259), and 42 μg packaging vector psPAX2 (Addgene# 12260) using transfection reagent lipofectamine 2000 with PLUS reagent (Thermo Fisher Scientific) according to manufacturer's manual. Six hours post transfection, the media was replenished with 27 mL of antibiotic-free media, and the virus-containing supernatant was harvested 66 h post transfection, filtered with a 0.45 μm Steriflip filter unit (MilliporeSigma), aliquoted into 30 mL/tube, and stored at −80°C.

**Lentivirus MOI determination—**To determine the lentivirus volume required for the screen, we measured the virus titer by transducing the cells with a series of diluted virus

solution and calculating the cell viability after puromycin selection. In brief, the clonal cell line used in the screen was seeded in a 12-well plate at a density of $1 \times 10^5$ cells/well. The next day, 400 μL of virus stock was subjected to a 2-fold serial dilution, up to a total of 8 dilutions. Each diluted virus solution was applied into a well containing 400 μL media supplemented with 16 μg/mL polybrene (MilliporeSigma), and a mock-infected well was included as a control. After 24 h, cells in each well were trypsinized and split into two replicated wells in a 6-well plate in the presence or absence of 0.5 μg/mL puromycin treatment. After 72 h, the cell viability was measured using CellTiter-Glo (Promega), and the multiplicity of infection (MOI) was calculated by dividing the luminescence of the well with puromycin to the well without puromycin. The titrated virus volume corresponding to MOI 0.3 was applied to the screen.

**Genome-wide CRISPR-Cas9 screen—**160 million HeLa cells carrying the reporter LBR1600*S11 and NLS-GFP1-10 were transduced with lentiviral Brunello library at MOI 0.3 in the presence of 8 μg/mL polybrene, in which each sgRNA had approximately 600 represented cells. After 24 h, cells were trypsinized and split 1:5 with media containing 0.5 μg/mL puromycin to remove the untransduced cells. After 4 days of selection, surviving cells were pooled and 100 million cells were maintained in fifty 15 cm plates, such that each sgRNA had at least 1000 represented cells in the population. The remaining cells were aliquoted into 100 million cells/tube and frozen, which served as a reference control of all representative sgRNAs in the library. Two days later, 0.5 μg/mL doxycycline was added to induce the reporter expression. After 24 h of induction, cells were pooled and an aliquot of 100 million cells was harvested prior to the sorting. This fraction serves as a reference control for the sgRNA enrichment analysis compared to the sorted population. Another 100 million cells were harvested and resuspended in sorting buffer (1 × Hank's balanced salt solution, 0.5% BSA, 25 mM HEPES, 2 mM EDTA) at a density of 8 million cells/mL. The cells were filtered through a 40 μm nylon mesh and sorted based on GFP intensity using a fluorescence-activated cell sorter (BD FACS Aria III). About 2.8 million (~3%) cells with the highest GFP signal were collected in $CO_2$-independent media supplemented with 50% FBS. The sorted cells were cultured for additional 5 days and subjected to the second round of sorting using the same gating strategy. Genomic DNA of the unsorted cells were extracted using Blood & Cell Culture DNA kit (Qiagen) with a Genome-Tip 500/G column, while the DNA of the sorted cells were purified using a Genome-Tip 20/G column according to manufacturer's protocol. sgRNA sequences were amplified from the purified genomic DNA via PCR using NEB Next High Fidelity PCR Master Mix (New England Biolabs) and NGS primers harboring Illumina TruSeq adaptor P5 and P7 according to the protocol described in.[60] The PCR amplicons were pooled and purified using Zymo-Spin V columns (Zymo Research), 5 μg of DNA was resolved on a 2% (w/v) agarose gel, and the library band sized 270–280 bp was cut out and purified using Qiagen gel extraction kit. The concentration and DNA size of individual library were determined using Bioanalyzer (Agilent), and libraries were pooled and sequencing on an Illumina NovaSeq platform at Yale Center for Genome Analysis. sgRNA paired-end reads were merged using QIIME v1.8.[59] sgRNA read counts with respect to the Brunello library were then determined using the Python script *count_spacers.py* from.[60] Gene rankings were generated by comparing the gene enrichment of high GFP cells to the unsorted cells using MAGeCK-VISPR v 0.5.4.[27,61]

**GO term enrichment analysis—**The Protein ANalysis THrough Evolutionary Relationships (PANTHER) classification system (http://geneontology.org/)[62,63] was used to perform the GO term enrichment analysis. Brunello library gene IDs and those genes identified by MAGeCK to have an RRA ≥ 5 were used as the reference and analysis gene sets, respectively. All other parameters of the classification system (test type, correction, etc.) were set to default. Enriched GO terms were identified for the GO biological process complete (BP), GO cellular component complete (CC), and GO molecular function complete (MF) categories. GO terms displayed in Figure S1 were selected as the top-level parent terms resulting from the PANTHER hierarchy sort and an FDR <0:05. GOnet (https://tools.dice-database.org/GOnet/)[64] GO-term-enrichment graphs were generated by providing genes identified by MAGeCK to have an RRA ≥5 and using the “biological_process” GO namespace and “Human” species parameters. All other parameters were left as default. To simplify the resulting GOnet graphs, a p-value threshold of ≤4:55e – 6 and Euler distances were used; unconnected terms were removed.

**Generation of CRISPR-Cas9 mediated knockout cell lines—**To validate hits identified from the CRISPR screen, we cloned three independent sgRNAs of each gene into lentiGuide-Puro plasmid (Addgene# 52963), the same plasmid backbone carrying the Brunello library. The cloning was performed as described in.[57] The reporter cell line was transduced with lentivirus carrying sgRNAs targeting to individual gene and selected by puromycin as described above. The knockout status of cells was confirmed via immunoblotting. Knockout cells were treated with 0.5 μg/mL doxycycline for 24 h and analyzed using a BD FACS LSR Fortessa X20 (BD Biosciences). Acquired data were processed using FlowJo software (FlowJo, LLC).

**Generation of endogenous tagging cell line using CRISPR-Cas12a—**RNF5, Ube2G2, and Ube2D3 were endogenously tagged with 3xHA at the C-terminus using the CRISPR Cas12a-assisted PCR tagging described.[42] Two gene-specific tagging oligos M1 and M2 harboring the homology arms were designed using tool at http://www.pcr-tagging.com; the gene specific cassette was generated via PCR using M1/M2 primers with template plasmids carrying the 3xHA tag and the puromycin resistance gene (Addgene# #120039). Wild-type HeLa cells were co-transfected with the PCR cassette and a plasmid encoding PAM specific endonuclease Cas12a (Addgene#89355 and #89353).[58] The cells were subjected to 0.5 μg/mL puromycin selection for 7 days, and a single clonal cell was isolated as described in previous section. Immunoblotting was used to confirm the endogenous tagging.

**Cycloheximide chase assay—**Cells were treated with 0.5 μg/mL doxycycline to induce the substrate expression for 24 h. The next day, cells were washed with PBS once and incubated with 100 μg/mL cycloheximide for the indicated time. At each time point, cells were harvested and frozen at −80°C. After all samples were collected, cells were lysed with 1 × sample buffer (50 mM Tris-HCl, pH 7.8, 4% SDS, benzonase 500 unit/mL), vortexed, and incubated at room temperature for 15 min. Lysate were heated at 65°C for 5 min, and 5 μg of lysates were subjected to an SDS-PAGE and immunoblotted with indicated antibodies. The images were quantified using Image J (Fiji),[65] and the LBR1600 signals

were normalized to the loading control GAPDH first, and further normalized to the signal of time-point zero in each set of samples. Time point zero was defined as 100%, and data was presented as % remaining at each time point.

**Immunofluorescence and image quantification—**Cells were seeded on a 15-mm round coverslip 24 h before transfection. The next day, cells were transfected with plasmids encoding the indicated proteins using Fugene HD (Promega) following manufacturer's protocol, and LBR1600*S11 was induced in the presence of 0.5 μg/mL doxycycline. After 24 h, immunofluorescence was performed as previously described.[21] In brief, cells were fixed with 4% paraformaldehyde/PBS for 15 min, washed with PBS 3 times, permeabilized with 0.1% Triton X-100/PBS for 10 min, and blocking with 5 mg/mL BSA for 30 min. The coverslips were then incubated with indicated primary antibodies prepared in 0.5% BSA/PBS at a dilution of 1:500 for 1 h. After washing with PBS 3 times, the coverslips were incubated with Alexa Fluor-conjugated secondary antibodies (ThermoFisher) at a dilution of 1:600 for another 1 h and followed by 3 times of PBS wash. Coverslips were stained with Hoechst (1 μg/mL) for 5 min and mounted onto microscope slides using Flouromount-G (Southern Biotech). The representative images were acquired using a confocal microscope (LSM 880 Airyscan, Zeiss). For endogenous RNF5-3HA, Ube2G2-3HA, and Ube2D3-3HA staining, the coverslips were blocked with 5% (v/v) donkey serum for 1 h, incubated with primary antibody mouse anti-HA (16B12) for 1 h, and then incubated with bridge antibody (goat-anti mouse) for 1 h, and finally with Alexa Flour-conjugated donkey anti-goat tertiary antibody for 1 h. All antibodies for bridge immunostaining were prepared in 5% (v/v) donkey serum/PBS.

For rescue experiments, the rescue ability of the overexpressed proteins was judged by monitoring LBR1600*S11 levels. About 100 cells transfected with rescue plasmid were imaged in each sample using an epifluorescence microscope (Observer D1, Zeiss). The fluorescence was quantified using Image J (Fiji). To make the quantification comparable among the transfected cells with varied expression, we sorted the cells based on the expression level of the expressed protein. Cells with very high expression (integrated density>50) or very low expression (integrated density<10) were not quantified. For cells with moderate expression of the rescue proteins (integrated density ranged from 10 to 50), the nucleus of the transfected cell was delineated in Hoechst staining channel first using the freehand tool of ImageJ, then the marked nuclear area was applied to the LBR1600* channel, and then the integrated density of the nuclear LBR1600* was measured and the value was copied and pasted to an Excel spreadsheet. We also quantified the LBR1600* fluorescence of 100 non-transfected cells on the same coverslip, and the LBR1600* signal was compared in transfected to non-transfected cells on the same coverslip. Statistical analysis was performed using a t-test (GraphPad Prism).

**Immunoprecipitation—**1.2 million cells were seeded on a 10 cm dish the day before transfection. At the second day, cells were transfected with 2.5 μg of indicated plasmids using lipofectamine 2000 (ThermoFisher) according to manufacturer's protocol. After 3 h of transfection, cells were replenished with fresh media including 0.5 μg/mL doxycycline and incubated overnight. Cells were lysed with 1 mL buffer (50 mM Tris-HCl, pH7.4, 0.5%

NP-40, 150 mM NaCl, 5 mM EDTA, and complete protease inhibitor cocktail (Roche)) and kept on ice with gently vortex every 2 min up to total 20 min. The lysates were centrifuged at 15,000 × g for 20 min at 4°C to pellet the cellular debris, and supernatant were transferred into new tubes and pre-cleared with 20 μL of protein A beads for 1 h at 4°C. After preclearing, the lysates were incubated with 0.05 μg of anti-LBR antibody and another 20 μL of protein A beads for 2 h. After 4 washes of lysis buffer, the beads were resuspended in 1 × sample buffer and heat at 65°C for 5 min. In the case of immunoprecipitation of HA or Flag tag, the lysates were directly incubated with 20 μL of HA or Flag beads for 2 h at 4°C.

**Ubiquitylation assay—**Cells were seeded on a 10 cm dish and transfected with plasmid encoding HA-Ubiquitin as described above. The cell pellets were lysed with 100 μL of 1% SDS/PBS containing benzonase 250 unit. Lysates were vortexed and incubated at room temperature for 20 min and diluted with 900 μL of buffer (50 mM Tris-HCl, pH 7.4, 0.5% NP-40, 150 mM NaCl, 10 mM NEM, 5 mM EDTA, and complete protease inhibitor cocktail). The lysates were centrifuged at 15,000× g for 20 min at 4°C and followed by immunoprecipitation performed as described above.

**SDS-PAGE and immunoblotting—**Gel electrophoresis used in this study was a 7% Tricine SDS-PAGE.[66] Proteins were transferred to a PVDF membrane (Bio-Rad) using buffer (20 mM Tris, 192 mM Glycine, and 10% methanol) at constant voltage 100V for 1 h at 4°C. The membrane was blocked with 5% (w/v) skim milk/PBS for 1 h, incubated with indicated primary antibody prepared in 1% (w/v) BSA/PBS-T (PBS with 0.05% (v/v) Tween 20) for 1 h, washed four times with PBS-T for 10 min, followed by incubation with HRP-conjugated secondary antibody for another 1 h, and again washed four times with PBS-T for 10 min. ECL (SuperSignal West Femto, Thermo Fisher Scientific) was used for visualization via photographic films or a ChemiDoc imaging system (Bio-Rad Laboratories). Image quantification was performed using Image J (Fiji).

**siRNA-mediated gene silencing—**The siRNA oligos used for silencing human RNF5 were described in.[51] Oligos were synthesized as complementary dsRNAs carrying the dTdT overhangs (Millipore-Sigma) at the 3′-ends of sequences targeting to RNF5 as follows: oligo#1: 5′-gcgcgaccttcgaatgtaa-3′, #2: 5′-cggcaagagtgtccagtat-3′). HRD1 depletion was conducted using an On-TargetPlus SMARTpool siRNA (Horizon discovery). The siRNA oligos were transfected into target cells using Lipofectamine RNAiMAX (Thermofisher) with a final siRNA concentration of 25 nM and incubated for 48 h.

**Polysome profiling—**Cytosolic lysates from the reporter cells and TMEM33 KO cells were subjected to polysome profiling analysis.[67] Briefly, 2 million cells were seeded in a 10 cm dish a day prior to harvesting. 10%–50% gradients were made by sequential overlays of 50%, 40%, 30%, 20%, and 10% sucrose solution prepared in salt buffer (20 mM Tris-HCl, pH 7.5, 100 mM NaCl, and 5 mM $MgCl_2$). The gradients were incubated at 4°C overnight before use. Prior to harvesting, cells were treated with 100 μg/mL CHX at 37°C for 10 min to stabilize polysomes, washed with cold PBS supplemented with 100 μg/mL CHX, scraped, and collected in a 15 mL tube. Cells were then pelleted at 500 × g for 5 min at 4°C and resuspend with 0.9 mL of polysome extraction buffer (20 mM Tris-HCl, pH 7.5,

100 mM KCl, 5 mM $MgCl_2$, 0.5% (v/v) NP-40, 1× EDTA-free protease inhibitor cocktail (Roche), RNase inhibitor 40U/μL (Promega), 100 μg/mL CHX) and transferred into a 1.5 mL tube. The lysates were incubated on ice for 10 min with tube inverting every 2 min and centrifuged at 12,000 ×g for 10 min at 4°C. 800 μL of supernatants were transferred into a new tube and RNA concentrations were determined by $OD_{A260}$. Equal amount of total RNA (290 μg) from each sample were loaded on top of the gradient, and centrifugated at 19,000 ×g (39,000 rpm) for 90 min at 4°C in a swinging-bucket rotor SW41Ti (Beckman). After centrifugation, each gradient was manually fractionated into 12 tubes starting from the top. 500 μL of solution from each fraction was applied for RNA extraction using Trizol reagent (ThermoFisher). Purified RNAs were then analyzed using RT-qPCR.

### QUANTIFICATION AND STATISTICAL ANALYSIS

Statistical analysis in this study were performed using GraphPad Prism 9. The significance of sample comparisons among different experimental groups was assessed using t test or one-way ANOVA. p-value $<0.05$ was considered statistically significant.

## Supplementary Material

Refer to Web version on PubMed Central for supplementary material.

## ACKNOWLEDGMENTS

This work is supported by NIH R01GM126835 to C.S. R.R.W. was funded by NIH T32 GM007499 and NIH F31 AR073094-01A1. We thank Christopher Richards and Jan Carette at Stanford University for discussion of the CRISPR screen, Morven Graham for help with electron microscopy, Yale Center for Genome Analysis for help with deep sequencing, and members of Schlieker lab for critical reading of the manuscript.

## REFERENCES

1. Bahmanyar S, and Schlieker C (2020). Lipid and protein dynamics that shape nuclear envelope identity. Mol. Biol. Cell 31, 1315–1323. 10.1091/mbc.E18-10-0636. [PubMed: 32530796]
2. Pawar S, and Kutay U (2021). The diverse cellular functions of inner nuclear membrane proteins. Cold Spring Harb. Perspect. Biol. 13, a040477. 10.1101/cshperspect.a040477. [PubMed: 33753404]
3. Gerace L, and Tapia O (2018). Messages from the voices within: regulation of signaling by proteins of the nuclear lamina. Curr. Opin. Cell Biol. 52, 14–21. 10.1016/j.ceb.2017.12.009. [PubMed: 29306725]
4. Shin JY, and Worman HJ (2022). Molecular pathology of laminopathies. Annu. Rev. Pathol. 17, 159–180. 10.1146/annurevpathol-042220-034240. [PubMed: 34672689]
5. Wu X, and Rapoport TA (2018). Mechanistic insights into ER-associated protein degradation. Curr. Opin. Cell Biol. 53, 22–28. 10.1016/j.ceb.2018.04.004. [PubMed: 29719269]
6. Lemberg MK, and Strisovsky K (2021). Maintenance of organellar protein homeostasis by ER-associated degradation and related mechanisms. Mol. Cell 81, 2507–2519. 10.1016/j.molcel.2021.05.004. [PubMed: 34107306]
7. Tsai PL, Zhao C, Turner E, and Schlieker C (2016). The Lamin B receptor is essential for cholesterol synthesis and perturbed by disease-causing mutations. Elife 5, e16011. 10.7554/eLife.16011. [PubMed: 27336722]
8. Buchwalter A, Schulte R, Tsai H, Capitanio J, and Hetzer M (2019). Selective clearance of the inner nuclear membrane protein emerin by vesicular transport during ER stress. Elife 8, e49796. 10.7554/eLife.49796. [PubMed: 31599721]

9. Christianson JC, and Carvalho P (2022). Order through destruction: how ER-associated protein degradation contributes to organelle homeostasis. EMBO J. 41, e109845. 10.15252/embj.2021109845. [PubMed: 35170763]
10. Mannino PJ, and Lusk CP (2022). Quality control mechanisms that protect nuclear envelope identity and function. J. Cell Biol. 221, e202205123. 10.1083/jcb.202205123. [PubMed: 36036741]
11. Boni A, Politi AZ, Strnad P, Xiang W, Hossain MJ, and Ellenberg J (2015). Live imaging and modeling of inner nuclear membrane targeting reveals its molecular requirements in mammalian cells. J. Cell Biol. 209, 705–720. 10.1083/jcb.201409133. [PubMed: 26056140]
12. Ungricht R, Klann M, Horvath P, and Kutay U (2015). Diffusion and retention are major determinants of protein targeting to the inner nuclear membrane. J. Cell Biol. 209, 687–703. 10.1083/jcb.201409127. [PubMed: 26056139]
13. Ohba T, Schirmer EC, Nishimoto T, and Gerace L (2004). Energy- and temperature-dependent transport of integral proteins to the inner nuclear membrane via the nuclear pore. J. Cell Biol. 167, 1051–1062. 10.1083/jcb.200409149. [PubMed: 15611332]
14. Khmelinskii A, Blaszczak E, Pantazopoulou M, Fischer B, Omnus DJ, Le Dez G, Brossard A, Gunnarsson A, Barry JD, Meurer M, et al. (2014). Protein quality control at the inner nuclear membrane. Nature 516, 410–413. 10.1038/nature14096. [PubMed: 25519137]
15. Foresti O, Rodriguez-Vaello V, Funaya C, and Carvalho P (2014). Quality control of inner nuclear membrane proteins by the Asi complex. Science 346, 751–755. 10.1126/science.1255638. [PubMed: 25236469]
16. Deng M, and Hochstrasser M (2006). Spatially regulated ubiquitin ligation by an ER/nuclear membrane ligase. Nature 443, 827–831. 10.1038/nature05170. [PubMed: 17051211]
17. Smoyer CJ, and Jaspersen SL (2019). Patrolling the nucleus: inner nuclear membrane-associated degradation. Curr. Genet. 65, 1099–1106. 10.1007/s00294-019-00971-1. [PubMed: 31020383]
18. Waterham HR, Koster J, Mooyer P, Noort Gv G.v., Kelley RI, Wilcox WR, Wanders RJA, Hennekam RCM, and Oosterwijk JC (2003). Autosomal recessive HEM/Greenberg skeletal dysplasia is caused by 3 beta-hydroxysterol delta 14-reductase deficiency due to mutations in the lamin B receptor gene. Am. J. Hum. Genet. 72, 1013–1017. 10.1086/373938. [PubMed: 12618959]
19. Turner EM, and Schlieker C (2016). Pelger-Huet anomaly and Greenberg skeletal dysplasia: LBR-associated diseases of cholesterol metabolism. Rare Dis. 4, e1241363. 10.1080/21675511.2016.1241363. [PubMed: 27830109]
20. Feng S, Sekine S, Pessino V, Li H, Leonetti MD, and Huang B (2017). Improved split fluorescent proteins for endogenous protein labeling. Nat. Commun. 8, 370. 10.1038/s41467-017-00494-8. [PubMed: 28851864]
21. Tsai PL, Zhao C, and Schlieker C (2019). Methodologies to monitor protein turnover at the inner nuclear membrane. Methods Enzymol. 619, 47–69. 10.1016/bs.mie.2018.12.033. [PubMed: 30910029]
22. Smoyer CJ, Katta SS, Gardner JM, Stoltz L, McCroskey S, Bradford WD, McClain M, Smith SE, Slaughter BD, Unruh JR, and Jaspersen SL (2016). Analysis of membrane proteins localizing to the inner nuclear envelope in living cells. J. Cell Biol. 215, 575–590. 10.1083/jcb.201607043. [PubMed: 27831485]
23. Ji Z, Li H, Peterle D, Paulo JA, Ficarro SB, Wales TE, Marto JA, Gygi SP, Engen JR, and Rapoport TA (2022). Translocation of polyubiquitinated protein substrates by the hexameric Cdc48 ATPase. Mol. Cell 82, 570–584.e8. 10.1016/j.molcel.2021.11.033. [PubMed: 34951965]
24. Ye Y, Meyer HH, and Rapoport TA (2001). The AAA ATPase Cdc48/p97 and its partners transport proteins from the ER into the cytosol. Nature 414, 652–656. 10.1038/414652a. [PubMed: 11740563]
25. Anderson DJ, Le Moigne R, Djakovic S, Kumar B, Rice J, Wong S, Wang J, Yao B, Valle E, Kiss von Soly S, et al. (2015). Targeting the AAA ATPase p97 as an approach to treat cancer through disruption of protein homeostasis. Cancer Cell 28, 653–665. 10.1016/j.ccell.2015.10.002. [PubMed: 26555175]

26. Doench JG, Fusi N, Sullender M, Hegde M, Vaimberg EW, Donovan KF, Smith I, Tothova Z, Wilen C, Orchard R, et al. (2016). Optimized sgRNA design to maximize activity and minimize off-target effects of CRISPR-Cas9. Nat. Biotechnol. 34, 184–191. 10.1038/nbt.3437. [PubMed: 26780180]
27. Li W, Xu H, Xiao T, Cong L, Love MI, Zhang F, Irizarry RA, Liu JS, Brown M, and Liu XS (2014). MAGeCK enables robust identification of essential genes from genome-scale CRISPR/Cas9 knockout screens. Genome Biol. 15, 554. 10.1186/s13059-014-0554-4. [PubMed: 25476604]
28. Kolde R, Laur S, Adler P, and Vilo J (2012). Robust rank aggregation for gene list integration and meta-analysis. Bioinformatics 28, 573–580. 10.1093/bioinformatics/btr709. [PubMed: 22247279]
29. Mueller B, Lilley BN, and Ploegh HL (2006). SEL1L, the homologue of yeast Hrd3p, is involved in protein dislocation from the mammalian ER. J. Cell Biol. 175, 261–270. 10.1083/jcb.200605196. [PubMed: 17043138]
30. Urade T, Yamamoto Y, Zhang X, Ku Y, and Sakisaka T (2014). Identification and characterization of TMEM33 as a reticulon-binding protein. Kobe J. Med. Sci. 60, E57–E65. [PubMed: 25612671]
31. Arhatte M, Gunaratne GS, El Boustany C, Kuo IY, Moro C, Duprat F, Plaisant M, Duval H, Li D, Picard N, et al. (2019). TMEM33 regulates intracellular calcium homeostasis in renal tubular epithelial cells. Nat. Commun. 10, 2024. 10.1038/s41467-019-10045-y. [PubMed: 31048699]
32. Savage AM, Kurusamy S, Chen Y, Jiang Z, Chhabria K, MacDonald RB, Kim HR, Wilson HL, van Eeden FJM, Armesilla AL, et al. (2019). tmem33 is essential for VEGF-mediated endothelial calcium oscillations and angiogenesis. Nat. Commun. 10, 732. 10.1038/s41467-019-08590-7. [PubMed: 30760708]
33. Liu F, Ma M, Gao A, Ma F, Ma G, Liu P, Jia C, Wang Y, Donahue K, Zhang S, et al. (2021). PKM2-TMEM33 axis regulates lipid homeostasis in cancer cells by controlling SCAP stability. EMBO J. 40, e108065. 10.15252/embj.2021108065. [PubMed: 34487377]
34. Lu LF, Zhang C, Li ZC, Zhou XY, Jiang JY, Chen DD, Zhang YA, Xiong F, Zhou F, and Li S (2021). A novel role of Zebrafish TMEM33 in negative regulation of interferon production by two distinct mechanisms. PLoS Pathog. 17, e1009317. 10.1371/journal.ppat.1009317. [PubMed: 33600488]
35. Fenech EJ, Lari F, Charles PD, Fischer R, Laétitia-Thézénas M, Bagola K, Paton AW, Paton JC, Gyrd-Hansen M, Kessler BM, and Christianson JC (2020). Interaction mapping of endoplasmic reticulum ubiquitin ligases identifies modulators of innate immune signalling. Elife 9, e57306. 10.7554/eLife.57306. [PubMed: 32614325]
36. Chadrin A, Hess B, San Roman M, Gatti X, Lombard B, Loew D, Barral Y, Palancade B, and Doye V (2010). Pom33, a novel transmembrane nucleoporin required for proper nuclear pore complex distribution. J. Cell Biol. 189, 795–811. 10.1083/jcb.200910043. [PubMed: 20498018]
37. Smoyer CJ, Smith SE, Gardner JM, McCroskey S, Unruh JR, and Jaspersen SL (2019). Distribution of proteins at the inner nuclear membrane is regulated by the Asi1 E3 ligase in Saccharomyces cerevisiae. Genetics 211, 1269–1282. 10.1534/genetics.119.301911. [PubMed: 30709848]
38. Casey AK, Chen S, Novick P, Ferro-Novick S, and Wente SR (2015). Nuclear pore complex integrity requires Lnp1, a regulator of cortical endoplasmic reticulum. Mol. Biol. Cell 26, 2833–2844. 10.1091/mbc.E15-01-0053. [PubMed: 26041935]
39. Kurosaki T, Popp MW, and Maquat LE (2019). Quality and quantity control of gene expression by nonsense-mediated mRNA decay. Nat. Rev. Mol. Cell Biol. 20, 406–420. 10.1038/s41580-019-0126-2. [PubMed: 30992545]
40. Soullam B, and Worman HJ (1993). The amino-terminal domain of the lamin B receptor is a nuclear envelope targeting signal. J. Cell Biol. 120, 1093–1100. 10.1083/jcb.120.5.1093. [PubMed: 7679672]
41. Pickart CM (2000). Ubiquitin in chains. Trends Biochem. Sci. 25, 544–548. 10.1016/s0968-0004(00)01681-9. [PubMed: 11084366]
42. Fueller J, Herbst K, Meurer M, Gubicza K, Kurtulmus B, Knopf JD, Kirrmaier D, Buchmuller BC, Pereira G, Lemberg MK, and Knop M (2020). CRISPR-Cas12a-assisted PCR tagging of mammalian genes. J. Cell Biol. 219, e201910210. 10.1083/jcb.201910210. [PubMed: 32406907]

43. Chassé H, Boulben S, Costache V, Cormier P, and Morales J (2017). Analysis of translation using polysome profiling. Nucleic Acids Res. 45, e15. 10.1093/nar/gkw907. [PubMed: 28180329]
44. Guttman M, Russell P, Ingolia NT, Weissman JS, and Lander ES (2013). Ribosome profiling provides evidence that large noncoding RNAs do not encode proteins. Cell 154, 240–251. 10.1016/j.cell.2013.06.009. [PubMed: 23810193]
45. Fang S, Ferrone M, Yang C, Jensen JP, Tiwari S, and Weissman AM (2001). The tumor autocrine motility factor receptor, gp78, is a ubiquitin protein ligase implicated in degradation from the endoplasmic reticulum. Proc. Natl. Acad. Sci. USA 98, 14422–14427. 10.1073/pnas.251401598. [PubMed: 11724934]
46. Lilley BN, and Ploegh HL (2005). Multiprotein complexes that link dislocation, ubiquitination, and extraction of misfolded proteins from the endoplasmic reticulum membrane. Proc. Natl. Acad. Sci. USA 102, 14296–14301. 10.1073/pnas.0505014102. [PubMed: 16186509]
47. Christianson JC, Olzmann JA, Shaler TA, Sowa ME, Bennett EJ, Richter CM, Tyler RE, Greenblatt EJ, Harper JW, and Kopito RR (2011). Defining human ERAD networks through an integrative mapping strategy. Nat. Cell Biol. 14, 93–105. 10.1038/ncb2383. [PubMed: 22119785]
48. Younger JM, Chen L, Ren HY, Rosser MFN, Turnbull EL, Fan CY, Patterson C, and Cyr DM (2006). Sequential quality-control checkpoints triage misfolded cystic fibrosis transmembrane conductance regulator. Cell 126, 571–582. 10.1016/j.cell.2006.06.041. [PubMed: 16901789]
49. Kuan YC, Takahashi Y, Maruyama T, Shimizu M, Yamauchi Y, and Sato R (2020). Ring finger protein 5 activates sterol regulatory element-binding protein 2 (SREBP2) to promote cholesterol biosynthesis via inducing polyubiquitination of SREBP chaperone SCAP. J. Biol. Chem. 295, 3918–3928. 10.1074/jbc.RA119.011849. [PubMed: 32054686]
50. Zhong B, Zhang Y, Tan B, Liu TT, Wang YY, and Shu HB (2010). The E3 ubiquitin ligase RNF5 targets virus-induced signaling adaptor for ubiquitination and degradation. J. Immunol. 184, 6249–6255. 10.4049/jimmunol.0903748. [PubMed: 20483786]
51. Zhong B, Zhang L, Lei C, Li Y, Mao AP, Yang Y, Wang YY, Zhang XL, and Shu HB (2009). The ubiquitin ligase RNF5 regulates antiviral responses by mediating degradation of the adaptor protein MITA. Immunity 30, 397–407. 10.1016/j.immuni.2009.01.008. [PubMed: 19285439]
52. Ungricht R, and Kutay U (2017). Mechanisms and functions of nuclear envelope remodelling. Nat. Rev. Mol. Cell Biol. 18, 229–245. 10.1038/nrm.2016.153. [PubMed: 28120913]
53. Zargari A, Boban M, Heessen S, Andréasson C, Thyberg J, and Ljungdahl PO (2007). Inner nuclear membrane proteins Asi1, Asi2, and Asi3 function in concert to maintain the latent properties of transcription factors Stp1 and Stp2. J. Biol. Chem. 282, 594–605. 10.1074/jbc.M609201200. [PubMed: 17085444]
54. Boban M, Zargari A, André asson C, Heessen S, Thyberg J, and Ljungdahl PO (2006). Asi1 is an inner nuclear membrane protein that restricts promoter access of two latent transcription factors. J. Cell Biol. 173, 695–707. 10.1083/jcb.200601011. [PubMed: 16735580]
55. Natarajan N, Foresti O, Wendrich K, Stein A, and Carvalho P (2020). Quality control of protein complex assembly by a transmembrane recognition factor. Mol. Cell 77, 108–119.e9. 10.1016/j.molcel.2019.10.003. [PubMed: 31679820]
56. Khateb A, Deshpande A, Feng Y, Finlay D, Lee JS, Lazar I, Fabre B, Li Y, Fujita Y, Zhang T, et al. (2021). The ubiquitin ligase RNF5 determines acute myeloid leukemia growth and susceptibility to histone deacetylase inhibitors. Nat. Commun. 12, 5397. 10.1038/s41467-021-25664-7. [PubMed: 34518534]
57. Sanjana NE, Shalem O, and Zhang F (2014). Improved vectors and genome-wide libraries for CRISPR screening. Nat. Methods 11, 783–784. 10.1038/nmeth.3047. [PubMed: 25075903]
58. Gao L, Cox DBT, Yan WX, Manteiga JC, Schneider MW, Yamano T, Nishimasu H, Nureki O, Crosetto N, and Zhang F (2017). Engineered Cpf1 variants with altered PAM specificities. Nat. Biotechnol. 35, 789–792. 10.1038/nbt.3900. [PubMed: 28581492]
59. Caporaso JG, Kuczynski J, Stombaugh J, Bittinger K, Bushman FD, Costello EK, Fierer N, Peña AG, Goodrich JK, Gordon JI, et al. (2010). QIIME allows analysis of high-throughput community sequencing data. Nat. Methods 7, 335–336. 10.1038/nmeth.f.303. [PubMed: 20383131]

60. Joung J, Konermann S, Gootenberg JS, Abudayyeh OO, Platt RJ, Brigham MD, Sanjana NE, and Zhang F (2017). Genome-scale CRISPR-Cas9 knockout and transcriptional activation screening. Nat. Protoc. 12, 828–863. 10.1038/nprot.2017.016. [PubMed: 28333914]

61. Li W, Köster J, Xu H, Chen CH, Xiao T, Liu JS, Brown M, and Liu XS (2015). Quality control, modeling, and visualization of CRISPR screens with MAGeCK-VISPR. Genome Biol. 16, 281. 10.1186/s13059-015-0843-6. [PubMed: 26673418]

62. Mi H, Ebert D, Muruganujan A, Mills C, Albou LP, Mushayamaha T, and Thomas PD (2021). PANTHER version 16: a revised family classification, tree-based classification tool, enhancer regions and extensive API. Nucleic Acids Res. 49, D394–D403. 10.1093/nar/gkaa1106. [PubMed: 33290554]

63. Mi H, Muruganujan A, Huang X, Ebert D, Mills C, Guo X, and Thomas PD (2019). Protocol Update for large-scale genome and gene function analysis with the PANTHER classification system (v.14.0). Nat. Protoc. 14, 703–721. 10.1038/s41596-019-0128-8. [PubMed: 30804569]

64. Pomaznoy M, Ha B, and Peters B (2018). GOnet: a tool for interactive Gene Ontology analysis. BMC Bioinf. 19, 470. 10.1186/s12859-018-2533-3.

65. Schindelin J, Arganda-Carreras I, Frise E, Kaynig V, Longair M, Pietzsch T, Preibisch S, Rueden C, Saalfeld S, Schmid B, et al. (2012). Fiji: an open-source platform for biological-image analysis. Nat. Methods 9, 676–682. 10.1038/nmeth.2019. [PubMed: 22743772]

66. Tsai PL, Chiou NT, Kuss S, Garcıá-Sastre A, Lynch KW, and Fontoura BMA (2013). Cellular RNA binding proteins NS1-BP and hnRNP K regulate influenza A virus RNA splicing. PLoS Pathog. 9, e1003460. 10.1371/journal.ppat.1003460. [PubMed: 23825951]

67. Panda AC, Martindale JL, and Gorospe M (2017). Polysome fractionation to analyze mRNA distribution profiles. Bio. Protoc. 7, e2126. 10.21769/BioProtoc.2126.

## Highlights

- RNF5 and HRD1 establish a bipartite surveillance system to act on INM proteins
- TMEM33 interacts with RNF5 and is required for RNF5 biosynthesis and function
- RNF5 traffics to the nucleus in response to changes of substrate levels at the INM
- RNF5 depends partly on Ube2D3 while HRD1 relies on Ube2G2 for LBR1600* degradation

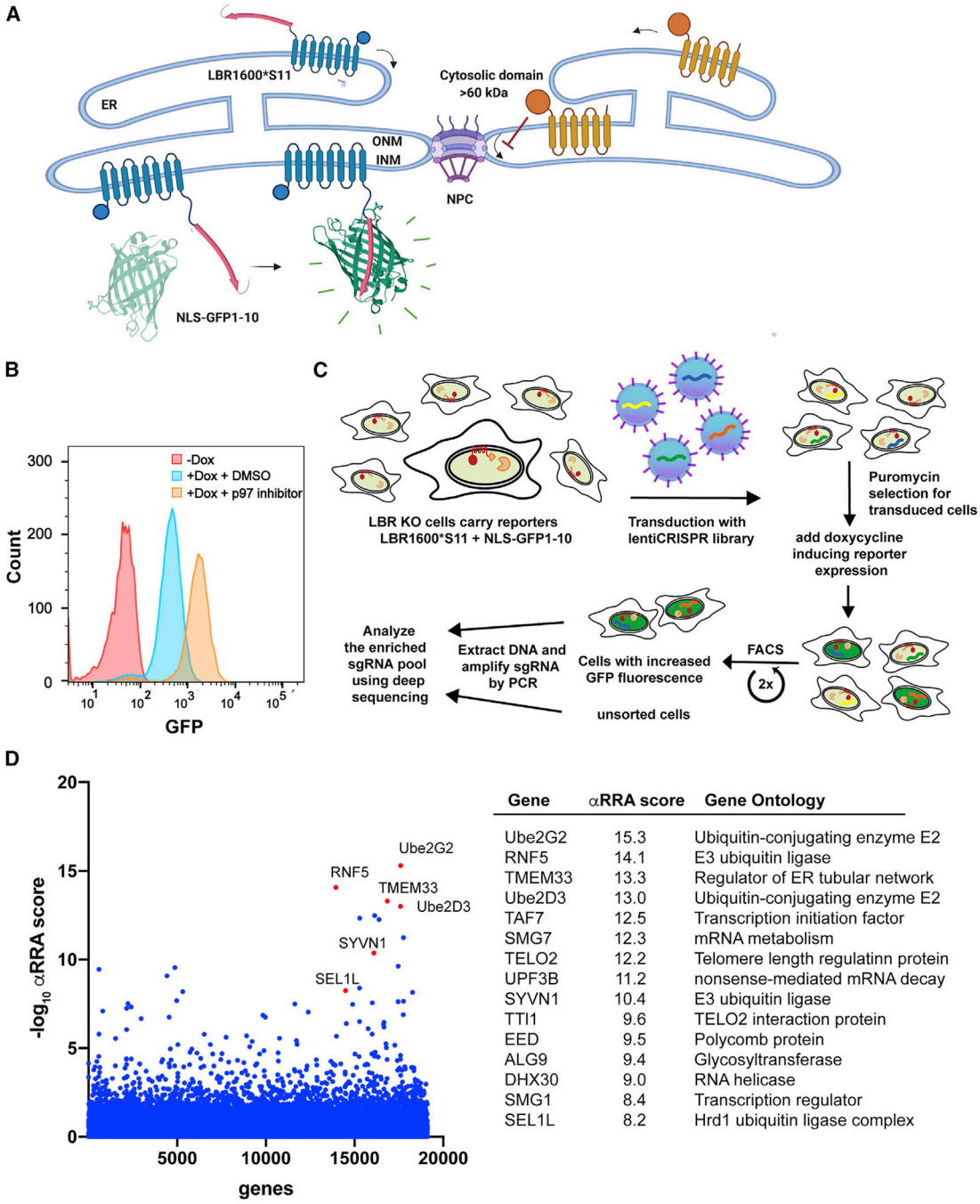


| Gene | αRRA score | Gene Ontology |
|---|---|---|
| Ube2G2 | 15.3 | Ubiquitin-conjugating enzyme E2 |
| RNF5 | 14.1 | E3 ubiquitin ligase |
| TMEM33 | 13.3 | Regulator of ER tubular network |
| Ube2D3 | 13.0 | Ubiquitin-conjugating enzyme E2 |
| TAF7 | 12.5 | Transcription initiation factor |
| SMG7 | 12.3 | mRNA metabolism |
| TELO2 | 12.2 | Telomere length regulatinn protein |
| UPF3B | 11.2 | nonsense-mediated mRNA decay |
| SYVN1 | 10.4 | E3 ubiquitin ligase |
| TTI1 | 9.6 | TELO2 interaction protein |
| EED | 9.5 | Polycomb protein |
| ALG9 | 9.4 | Glycosyltransferase |
| DHX30 | 9.0 | RNA helicase |
| SMG1 | 8.4 | Transcription regulator |
| SEL1L | 8.2 | Hrd1 ubiquitin ligase complex |

**Figure 1. A genome-wide screen identifies genes required for INM protein turnover**

(A) ER membrane proteins with large cytosolic domains cannot diffuse freely from the ER to the INM. Thus, a split-GFP system was employed to construct the LBR-based reporter for the screen. The C terminus of LBR1600* was fused to the last β strand of GFP that complements NLS-GFP1-10 lacking this C-terminal β strand, restoring GFP fluorescence in the nucleus. INM, inner nuclear membrane; ONM, outer nuclear membrane. GFP structure is adapted from PDB (2B3P).

(B) The reporter cell line was treated with doxycycline for 24 h, followed by 5 μM p97 inhibitor CB-5083 or DMSO for 3 h, and subjected to flow cytometry.
(C) Flowchart of the CRISPR screen. The reporter cell line was transduced with a lentiviral Brunello library, and cells with the highest GFP were enriched by two rounds of sorting at day 8 and day 13 post transduction.
(D) Candidate genes identified in the CRISPR screen. Gene significance was analyzed by comparing the gene enrichment in high-GFP cells with the unsorted population using the MAGeCK algorithm. The x axis corresponds to targeted genes in alphabetical order; y axis, significant enrichment of each gene represented as $-\mathrm{Log}_{10}$ robust rank aggregation (α-RRA). Gene ontology and the α-RRA score of the top-scoring 15 genes are listed in the table. See also Figure S1.

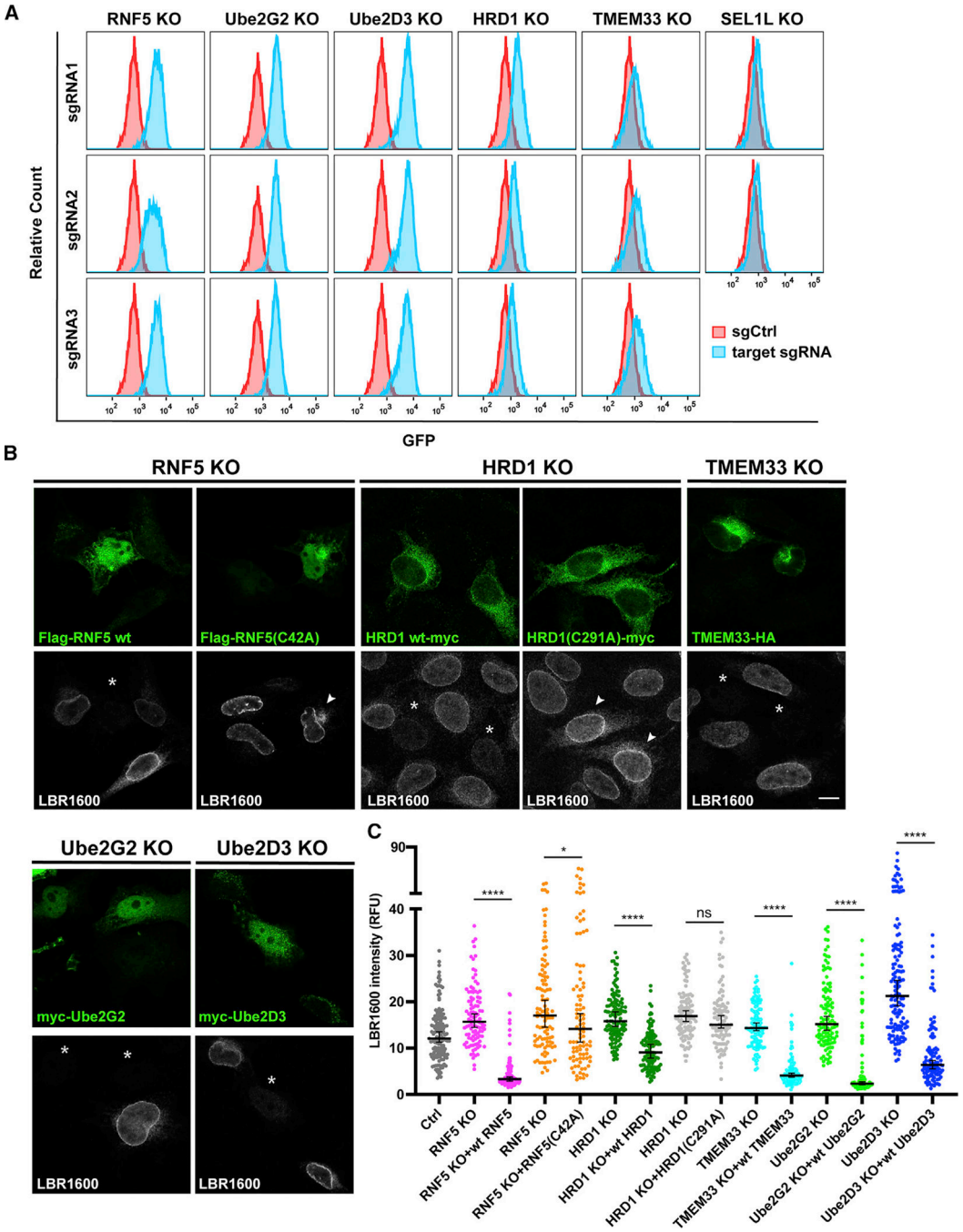


**Figure 2. Target validation of candidates involved in LBR1600*S11 turnover**

(A) Three independent sgRNAs utilized in the original Brunello library were used to generate KO cells for the indicated genes. KO cells were induced to express the LBR1600*S11 and NLS-GFP1-10 overnight and analyzed using flow cytometry. Parental cells transduced with non-targeting sgRNA were used as control.

(B) Representative confocal images of KO cells transfected with plasmids encoding corresponding WT proteins or ligase-inactive mutants to assess whether degradation of LBR1600*S11 can be rescued. Asterisks mark transfected cells devoid of LBR1600*S11;

arrowheads indicate transfected cells having similar LBR1600*S11 levels compared with non-transfected cells. Scale bar, 10 μm.

(C) Quantification of the rescuing ability determined by LBR1600*S11 fluorescence intensity. In each sample, about 100 transfected and non-transfected cells were quantified from three independent coverslips. Error bars indicate median with 95% confidence interval. p value was determined by t test. ****$p < 0.0001$; *$p < 0.05$; ns, not significant.

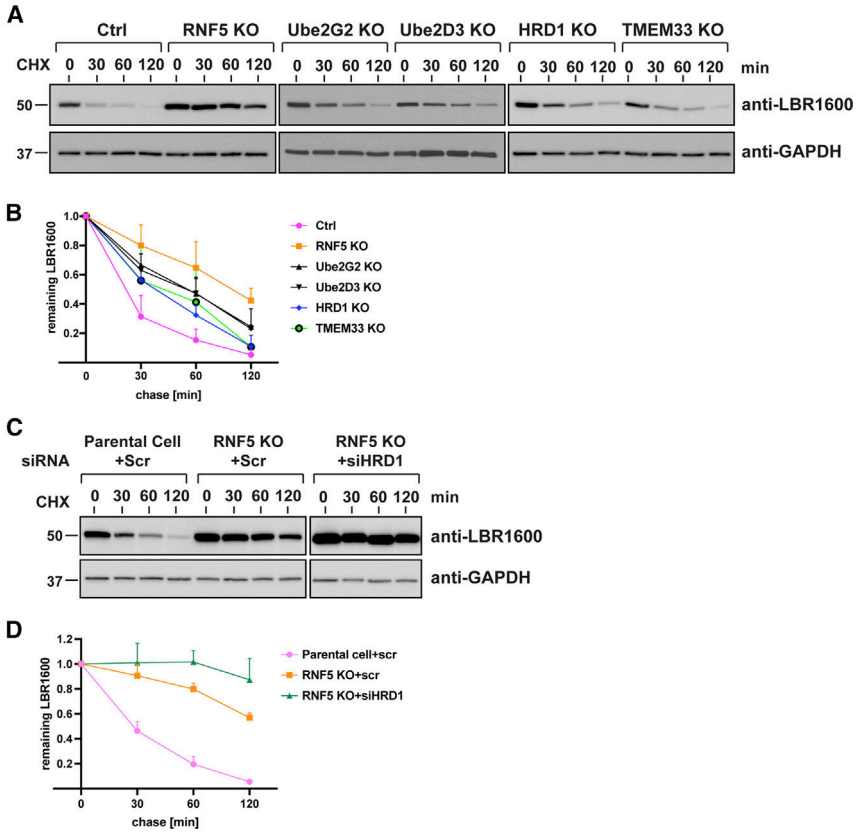


**Figure 3. Degradation of LBR1600* depends on the E3 ligases RNF5 and HRD1, TMEM33, and the E2 ubiquitin-conjugating enzymes, Ube2G2 and Ube2D3**

(A) LBR1600*S11 turnover was assessed in respective KO cells using a CHX-chase assay. Lysates from indicated time points were harvested and analyzed using immunoblotting.

(B) Quantification of CHX assay in (A) via densitometry. The plot shows the mean of three independent experiments ± SD.

(C) RNF5 KO cells were transfected with siRNAs for depleting HRD1 for 48 h, and CHX assays were performed as described in (A).

(D) Quantification of CHX assay in (C). The plot shows the mean of three independent experiments ±SD.

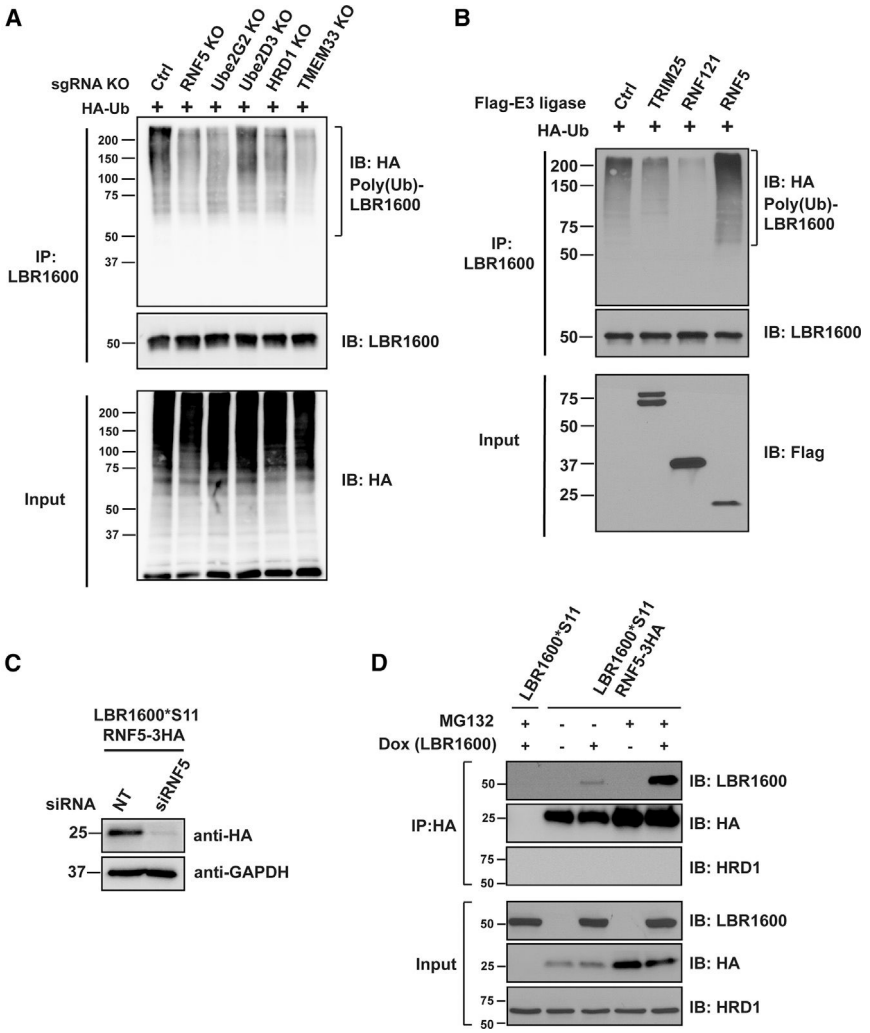


**Figure 4. RNF5, HRD1, TMEM33, Ube2G2, and Ube2D3 contribute to ubiquitylation of LBR1600***

(A) Reporter cell lines with the indicated KO condition were induced to express LBR1600*S11 and transfected with HA-ubiquitin, incubated for 24 h, and subjected to immunoprecipitation and immunoblotting using the indicated antibodies.

(B) FLAG-tagged E3 ligases and HA-ubiquitin were co-transfected into cells expressing LBR1600*S11, followed by immunoprecipitation and immunoblotting as in (A).

(C) The authentic RNF5 locus of the reporter cell line was tagged with HA, and validated by RNF5 depletion using siRNA and immunoblotting with anti-HA.

(D) Endogenous RNF5 interacts with LBR1600*S11. The reporter cell line with RNF5-HA expressed from the authentic locus was treated with or without doxycycline and MG132, followed by immunoprecipitation with anti-HA antibody and immunoblotting with the indicated antibodies. See also Figure S2.

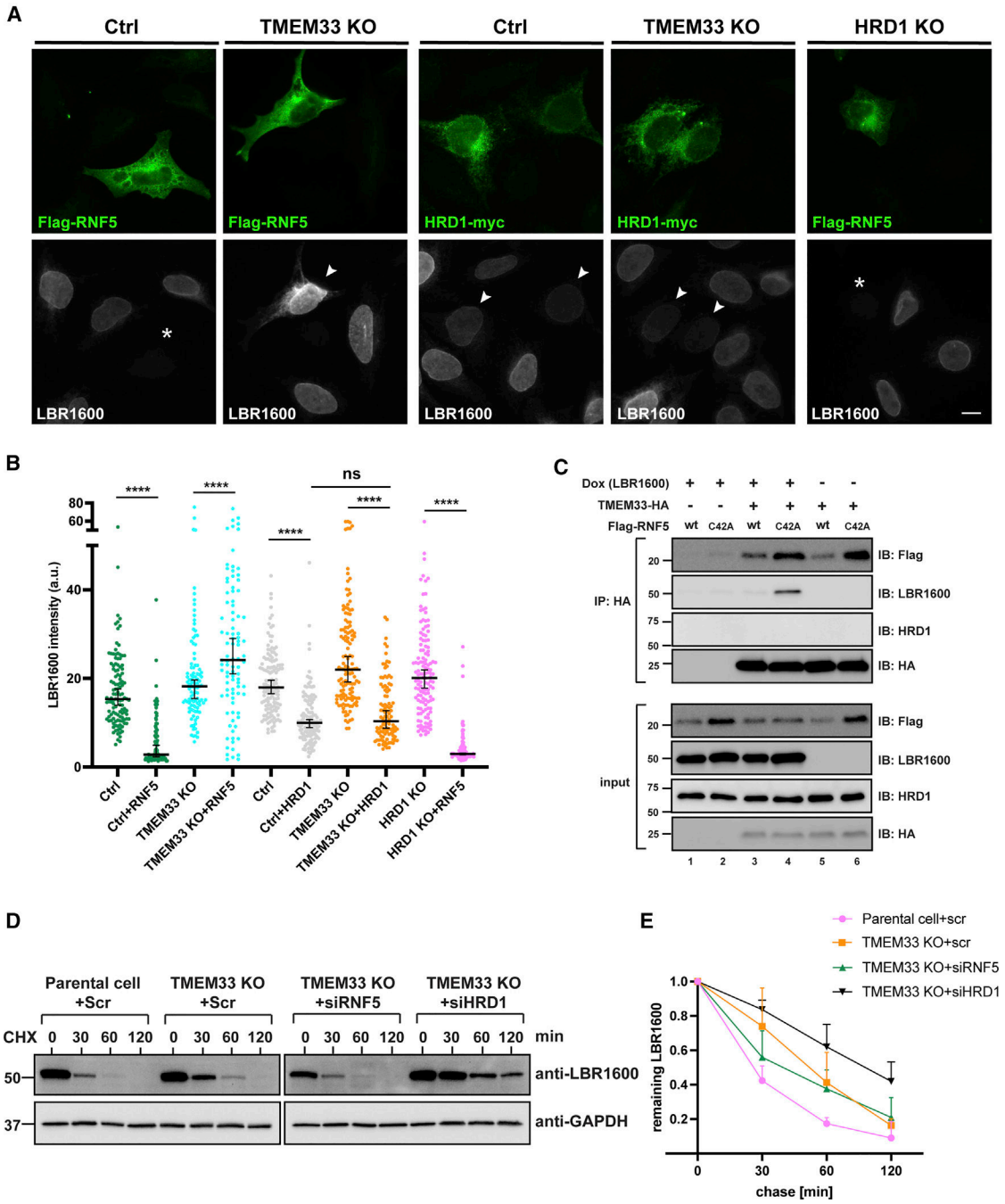


**Figure 5. Epistasis analysis of RNF5, TMEM33, and HRD1**

(A) FLAG-RNF5 or HRD1-myc were transiently expressed in WT, TMEM33 KO, or HRD1 KO cells expressing LBR1600*S11, followed by immunofluorescence microscopy using the indicated antibodies. Asterisks denote transfected cells devoid of LBR1600*S11; arrowheads indicate transfected cells with similar or moderate decreases in LBR1600*S11 levels compared with non-transfected cells. Scale bar, 10 μm.

(B) Quantification of RNF5 effect on LBR1600*S11 degradation in TMEM33 KO and HRD1 KO cells. Images were quantified as in Figure 2; about 100 cells with moderate

expression of FLAG-RNF5 were quantified in each sample. n = 100, N = 2. The plot shows median with 95% confidence interval. Data were analyzed using a t test. ****p <0.0001; ns, not significant.

(C) Cells expressing LBR1600*S11 were co-transfected with plasmids encoding TMEM33-HA and FLAG-RNF5 WT or FLAG-RNF5 C42A, lysed and subjected to immunoprecipitation with anti-HA beads, followed by immunoblotting using the indicated antibodies.

(D) Cycloheximide chase experiments were performed for the control or TMEM33 KO cells with the indicated siRNAs depleting RNF5 or HRD1.

(E) Quantification of the CHX assay in (D). The plot shows the mean of three independent experiments ±SD.

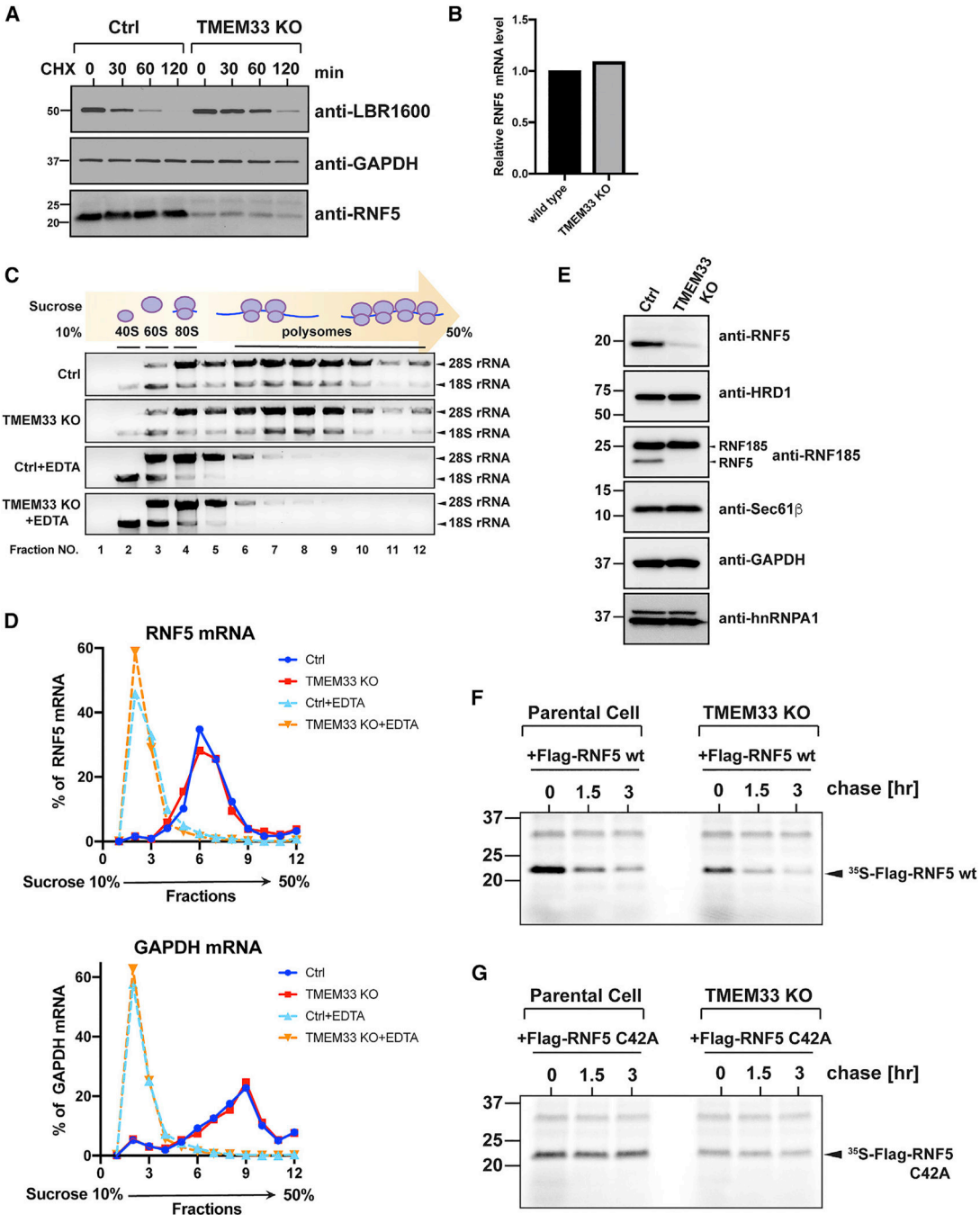


**Figure 6. TMEM33 is required for RNF5 biosynthesis**

(A) CHX-chase assay was performed to monitor the stability of the indicated proteins in reporter and TMEM33 KO cells.

(B) Relative mRNA levels of RNF5 were determined in control and TMEM33 KO cells using qPCR.

(C) Homogenates obtained from reporter and TMEM33 KO cells were treated with or without 30 mM EDTA and subjected to centrifugation over a 10%–50% sucrose gradient.

After ultracentrifugation, each gradient was fractionated, and RNAs were extracted and subjected to agarose gel electrophoresis.

(D) RNA isolates from (C) were subjected to RT-qPCR. The distribution of mRNA along the gradient is represented as percentage of total mRNA.

(E) Detergent extracts from reporter and TMEM33 KO cells were resolved by SDS-PAGE, followed by immunoblotting with indicated antibodies. Note that the anti-RNF185 antibody cross-reacts with RNF5 due to sequence similarity between those E3s.

(F) The reporter cells and TMEM33 KO cells were transfected with FLAG-RNF5 WT, metabolically labeled with $^{35}$S-Cys/Met for 5 min, and chased in the presence of excess unlabeled Cys/Met. FLAG-RNF5 was retrieved from lysates harvested at the indicated time points via immunoprecipitation, resolved by SDS-PAGE, and visualized by autoradiography.

(G) The reporter cells and TMEM33 KO cells transfected with FLAG-RNF5 C42A were subjected to pulse-chase analysis as described in (F).

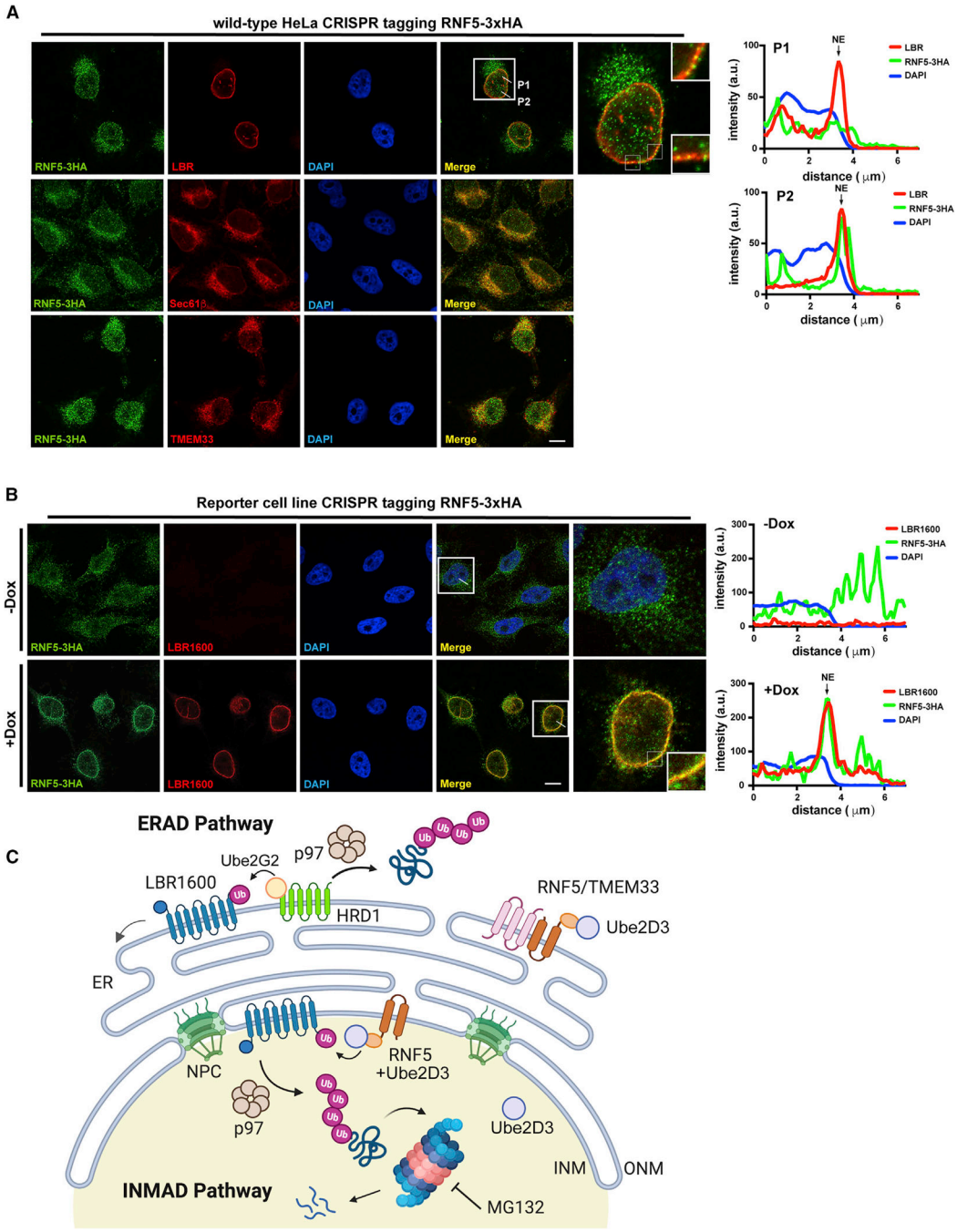


**Figure 7. RNF5 relocalizes to the NE upon LBR1600*S11 induction**

(A) RNF5 of WT HeLa cells was tagged with 3xHA at the endogenous locus and co-stained with antibodies against HA and LBR (as INM marker) or Sec61β or TMEM33 (as ER markers). The white box marks the representative cell enlarged in the last panel. White lines mark the position of the line-scan profile of the fluorescence intensity of RNF5-3xHA (green), LBR (red), and DNA (blue) across the NE. Scale bar, 10 μm.

(B) Reporter cell line with endogenously HA-tagged RNF5 was incubated with or without doxycycline for 24 h before immunofluorescence. Cells were co-stained with antibodies

against HA and LBR1600*S11. White boxes denoted the enlarged area in the last panel and the white lines correspond to the line-scan profile as described in (A). Scale bar, 10 μm. Note that the anti-LBR antibody can recognize both WT LBR and LBR1600*S11; however, since this cell line is an LBR KO genetic background, LBR signal is not observed in the absence of doxycycline.

(C) Proposed model of INM protein turnover. LBR1600* is synthesized at the ER and traffics along the ER membrane to the outer nuclear membrane (ONM) and inner nuclear membrane (INM), where it associates with the nuclear lamina and chromatin. A subset of misfolded LBR1600* is recognized by HRD1/Ube2G2 or RNF5-mediated ERAD and retrotranslocated into cytosol for degradation, whereas LBR1600* escaping ERAD is ubiquitylated by INM-resident RNF5/Ube2D3 and degraded in the nucleus through the action of p97 and the proteasome. See also Figures S3–S5 and S7.

## KEY RESOURCES TABLE

| REAGENT or RESOURCE |
| --- |
| Antibodies |
| Rabbit monoclonal anti-LBR clone E398L |
| Rabbit monoclonal anti-Ube2G2 clone EPR9248(2) |
| Rabbit monoclonal anti-RNF185 (EPR14070-94) |
| Mouse monoclonal anti-hnRNPA1 clone 9H10 |
| Mouse monoclonal anti-GAPDH |
| Mouse monoclonal anti-RNF5 (22B3) |
| Rabbit polyclonal anti-RNF5 |
| Rabbit polyclonal anti-TMEM33 |
| Rabbit monoclonal anti-SYVN1 clone D3O2A |
| Rabbit monoclonal anti-UbcH5C clone D60E2 |
| Mouse monoclonal anti-Lamin A/C clone 4C11 |
| Rabbit monoclonal anti-HA clone C29F4 |
| Rat monoclonal anti-HA clone 3F10 |
| Rat monoclonal antibody (clone 3F10) conjugated with peroxidase |
| Rat monoclonal anti-HA clone 3F10 affinity matrix |
| Mouse monoclonal anti-HA clone 16B12 |
| Mouse monoclonal anti-Flag clone M2 |

| REAGENT or RESOURCE |
| --- |
| Rabbit monoclonal anti-Flag clone D6W5B |
| Mouse monoclonal anti-myc clone 9E10 |
| Rabbit polyclonal anti-sec61b |
| Goat anti-mouse IgG (H + L) secondary antibody Alexa Fluor 568 |
| Goat anti-rabbit IgG (H + L) secondary antibody Alexa Fluor 647 |
| Goat Anti-Mouse IgG(H + L), Multi-Species SP ads-HRP |
| Goat Anti-Rabbit IgG(H + L), Mouse/Rat/Human ads-HRP |
| Peroxidase IgG Fraction Monoclonal Mouse Anti-Rabbit IgG, light chain specific |
| Peroxidase AffiniPure Goat Anti-Mouse IgG, light chain specific |
| AffiniPure Goat Anti-Mouse IgG (H + L) |
| Donkey Anti-Rabbit IgG (H + L) Alexa Fluor 594 |
| Donkey Anti-goat IgG (H + L) Alexa Fluor 488 |
| Donkey Anti-goat IgG (H + L) Alexa Fluor 647 |
| Bacterial and virus strains |
| Endura ElectroCompetent Cells |
| Chemicals, peptides, and recombinant proteins |
| P97 inhibitor, CB-5083 |
| MG132 |
| Geneticin Selective Antibiotic (G418 Sulfate) |
| Puromycin dihydrochloride |
| Hygromycin B |
| Doxycycline |
| Polybrene |
| Benzonase nuclease |

| REAGENT or RESOURCE |
|---|
| Cycloheximide |
| N-Ethylmaleimide (NEM) |
| DMEM media |
| Heat-inactivated Fetal Bovine Serum |
| Penicillin/streptomycin |
| Hank's balanced salt solution |
| Lipofectamine 2000 Transfection Reagent |
| PLUS reagent |
| Lipofectamine RNAiMAX Transfection Reagent |
| Fugene HD Transfection Reagent |
| NEB Next High Fidelity PCR Master Mix (2X) |
| Flouromount-G |
| Complete protease inhibitor cocktail |
| Nonidet P40 Substitute (NP-40) |
| SuperSignal West Femto Maximum Sensitivity Substrate |
| RNasin Plus Ribonuclease Inhibitor |
| TRIzol Reagent |
| SuperScript II Reverse Transcriptase |
| iQ SYBR Green Supermix |
| Critical commercial assays |
| Blood and Cell culture DNA kit, Genomic-tip 500/G |
| Blood and Cell culture DNA kit, Genomic-tip 20/G |
| Plasmid Maxi kit |
| CellTiter-Glo Luminescent Cell Viability Assay |
| Deposited data |
| Raw NGS results of the CRISPR screen |
| Experimental models: Cell lines |
| HeLa cell |
| 293T cell |
| Oligonucleotides |

| REAGENT or RESOURCE |
| --- |
| human RNF5-3xHA PCR tagging primer M1: GATCTGGGACAGGGTCACCCAGCCTCCAGCTGGCAGGATTCCCTCTTCCTGTTTCTCGCCATCTTCTTCTTTTTTTGGCTGCTCAGTATTTCAGGTGGAGGAGGTAG |
| human RNF5-3xHA PCR tagging primer M2: GGACCCTCAATACTGATTCTTCTCTGGCTGGAGGTGGGCAGGAAGCAGACATAGCAAAAAATAGCTCAAATACTGAGCAGCATCTACACTTAGTAGAAATTAGCTAC |
| human Ube2G2-3xHA PCR tagging primer M1: GCTAACGTGGATGCGTCCAAAATGTGGCGCGATGACCGGGAGCAGTTCTATAAGATTGCCAAGCAGATCGTCCAGAAGTCTCTGGGACTGTCAGGTGGAGGAGGT |
| human Ube2G2-3xHA PCR tagging primer M2: GGGGGAGAATGCTGAGCTGCTTGGCGGTGTGTGCGCGCCTGTGCGAGGCCAGGTCAAAAAAGGCCAGGTCTCACAGTCCCAATCTACACTTAGTAGAAATTAGCT |
| human Ube2D3-3xHA PCR tagging primer M1: TAGGAATTCTTTATTTTAACTTTTAAAAATAACATCTTTATTTACAGGTACAACAGAATATCTCGGGAATGGACTCAGAAGTATGCCATGTCAGGTGGAGGAGGTAGT |
| human Ube2D3-3xHA PCR tagging primer M2: GTAATTTAAAGTTTATTCCAGCTATAATGCAGGTTATTCTGACTTTAAGGTAGCAAAAAAATTTAAGGTAGCATCACATGGATCTACAAGAGTAGAAATTAGCTAGCT |
| qPCR primers of human RNF5: Forward: CCGGAGAGCAGAGGGGGATT |
| qPCR primers of human RNF5: Reverse: TGGGCATTGAAGACGGTGGT |
| qPCR primers of human GAPDH: Forward: CGACCGGAGTCAACGGATTTGGTCG |
| qPCR primers of human GAPDH: Reverse: GGCAACAATATCCACTTTACCAGA |
| Recombinant DNA |
| Retro-X Tet-On Inducible Expression System |
| Human sgRNA library Brunello in lentiGuide-Puro |
| lentiCas9-Blast |
| VSV-G envelope expressing plasmid pMD2.G |
| Lentiviral packaging vector psPAX2 |
| lentiGuide-Puro plasmid |
| PMaCTag-P28 (template for PCR tagging with 3xHA) |
| pcDNA3.1-hLbCpf1(TYCV) (for PCR tagging of RNF5 and Ube2G2) |
| pcDNA3.1-hAsCpf1(TATV) (for PCR tagging of Ube2D3) |
| pcDNA3-Flag-RNF5 |
| pcDNA3-Flag-RNF5(C42A) |
| pcDNA3-Hrd1wt-myc |
| pcDNA3-Hrd1(C291A)-myc |
| pcDNA3-TMEM33-HA |
| Software and algorithms |
| QIIME v1.8 |
| Python script *count_spacers.py* |
| MAGeCK-VISPR v 0.5.4 |

| REAGENT or RESOURCE |
| --- |
| PANTHER |
| GOnet |
| Fiji |
| FlowJo |
| Graphpad Prism 9 |